CR-54475

A MAGNETOGASDYNAMIC POWER GENERATION STUDY

Summary Report

Contract NAS 3-6260

prepared for

NATIONAL AERONAUTICS AND SPACE ADMINISTRATION

SPACE SCIENCES LABORATORY

GENERAL ELECTRIC

MISSILE AND SPACE DIVISION

Requests for copies of this report should be referred to

National Aeronautics and Space Administration
Office of Scientific and Technical Information
Attention: AFSS-A
Washington, D. C. 20546

GENERAL ELECTRIC
COMPANY

VALLEY FORGE SPACE TECHNOLOGY CENTER (MAIL: P. O. BOX 8555, PHILA., PA. 19101) . . TEL. 969-2000

MISSILE AND
SPACE DIVISION

SPACE SCIENCES
LABORATORY

February 10, 1966

Subject: Contract NAS 3-6260
Summary Report, NASA CR-54475

The enclosed document, "A Magnetogasdynamic Power Generation Study," is a summary report for the subject contract. It is sent for your perusal and retention in accordance with the distribution list furnished by NASA headquarters.

Very truly yours,

John H. Wood

John H. Wood
Senior Technical Editor

JHW/mjp

NASA CR-54475

SUMMARY REPORT

A MAGNETOGASDYNAMIC POWER GENERATION STUDY

Principal Investigator: F. H. Shair

Technical Direction: A. Sherman

prepared for

NATIONAL AERONAUTICS AND SPACE ADMINISTRATION

January 20, 1966

CONTRACT NAS 3-6260

Technical Management

NASA Lewis Research Center

Spacecraft Technology Division

Cleveland, Ohio

N. J. Stevens

GENERAL ELECTRIC COMPANY

Missile and Space Division

Space Sciences Laboratory

P.O. Box 8555, Philadelphia, Pa., 19101

ABSTRACT

16138

Experiments were performed with an electron beam to increase the electrical conductivity of a cesium-seeded argon plasma above the thermal equilibrium value in a subsonic duct at neutral particle temperatures up to 1500°K and pressures of the order of one atmosphere. Microwave interferometer diagnostic techniques indicated an electron density up to twenty times the Saha equilibrium value and a low electron density recombination rate which was supported, in qualitative trends at least, by theoretical analysis.

Other subsonic experiments conducted with applied electric and magnetic fields and using cesium and cesium-mercury (Penning) seed mixture indicated the existence of low net induced voltages, while experiments with only applied electric fields showed the influence of several types of cathode material and a relatively insensitive dependence of performance on seeding rate.

Intended experiments in a supersonic channel were prevented by equipment and materials problems which produced excessive contamination.

Calculations were also performed to determine the seed concentration required to obtain the optimum electrical conductivity for a MHD generator operating in the non-equilibrium mode. The results indicated a reduction in the seed concentration as compared to the equilibrium situation.

Author

TABLE OF CONTENTS

I. SUMMARY

Experiments were performed with an electrom beam to increase the electrical conductivity of a cesium seeded argon plasma in a dense alumina 1 cm x 3 cm duct at neutral gas temperatures up to 1500°K, Mach number up to 0.6 and a pressure of ~ 1-1/2 atmospheres. A typical argon mass flow rate in this range of operating conditions was 75 grms/sec. The electron beam was injected through a 0.25 mil aluminum foil window, an average current entering the plasma being 0.1 mA at 15,000-20,000 volts.

A 60 KMC microwave interferometer was used to measure electron densities with the following results:

1. electron densities over a small range of neutral gas temperature were 10 to 20 times the Saha equilibrium value, and

2. a slow electron density decay rate (due to a relatively low electron density level) was inferred and presumably gave rise to a measure of partially frozen ionization.

For this latter result, good agreement in the qualitative trends was obtained with the predictions of a recombination theory after making adjustments to the magnitude of the electron-ion pair production energy. These experiments generally confirmed the results of earlier work under a preceding contract.

Further subsonic channel experiments with applied electric and magnetic fields using cesium seed and a cesium-mercury (Penning) mixture showed that the net induced voltage reached only 8.7% of the theoretically attainable value of 28.8 volts. Compared with pure cesium, the Penning mixture inhibited the initial flow of current, but it is possible that its use produced significant volumetric ionization. In experiments with only applied electric fields, a barium oxide cathode was considerably superior in performance compared with 2% thoriated tungsten, while plain molybdenum was a fairly acceptable possibility. Cathode heating through ionic bombardment was definitely beneficial to performance, but the lowest zero current sheath loss (barium oxide cathode) was still high at 10 volts, and during experiments with other cathode materials this quantity ranged up to 44 volts. An associated preliminary result suggested that an order of magnitude variation (~ 0.1 to ~1% molar fraction) in cesium seed concentration (molybdenum cathode) had very little effect on performance.

The 2 cm x 3 cm dense alumina supersonic channel produced an exit centerline Mach number $\mathcal{M}$ = 1.80, the increase over the required design value of $\mathcal{M}$ = 1.50 being due to slight over-correction for viscous effects. Subsequent equipment and materials problems and the ensuing

contamination prevented the gathering of useful supersonic data during the contract period covered by this report.

Theoretical calculations of the seed concentration to produce a maximum conductivity were computed for a magnetically induced non-equilibrium MHD generator. The ratio of the equilibrium to non-equilibrium electron concentration was found to be relatively independent of gas temperature, gas pressure, or cross-section magnitude and of order of 10.

II. INTRODUCTION

A theoretically attractive solution to the problem of producing an electrical generator for space applications lies in the coupling of a plasma MGD device to a nuclear energy source. The basic requirement in the theoretical treatment of this type of plasma MGD generator is the successful inducement and maintenance of an appreciable conductivity when operating at a temperature level ($\leq 1500^{\circ}$ K) which is compatible with the operation of the nuclear reactor. Thermal equilibrium ionization at such total temperatures in a high speed flow system are several orders of magnitude too low for acceptable efficiency. Although there are many reported observations of the existence of non-equilibrium ionization (for example, references 1, 2 and 3), continuous power extraction at a significant level using this phenomenon has yet to be reliably demonstrated by experiment.

This report is concerned principally with the investigation of generating power from a cesium-seeded argon plasma. This choice of working fluid provides considerable experimental convenience and, from the MGD point of view, has many potential optimal qualities such as high conductivity and low cathode sheath voltage. These and other properties have been recently reported by Ellington(4) who investigated several seed and monatomic gas combinations in a static diode experiment. Before significant power can be generated in the non-equilibrium ionization regime, sufficiently high open circuit voltages must be induced to overcome the sheath voltages that develop: so far, measured open circuit voltages have reached only a modest fraction of the theoretically attainable value, with the result that power extraction has been several orders of magnitude below the expected.

III. OBJECTIVE AND SCOPE OF WORK

The present work is the continuation of a study* (5) in a 1 cm. x 3 cm. subsonic duct in which an electron beam was used to produce a plasma conductivity of approximately 10 mho/m, representing an approximate two order of magnitude increase over the Saha equilibrium value. In the same study, open circuit voltages reached a maximum of 25% of the theoretical value.

In addition to further investigation of the subsonic duct, experiments were to be performed in a 2 cm. x 3 cm. supersonic duct in order to elucidate the problems to be solved for the design of an efficient generator. These included electrode phenomena such as geometry and temperature, seed concentration requirement, and the effectiveness of pre-ionization techniques. The remaining experimental variables were to be magnetic field strength (approximately 20,000 gauss maximum), gas velocity (300 - 800 m/sec.), gas stagnation temperature (1000 - 1700°K) and seed material (cesium, mercury and cesium-mercury mixture). Microwave interferometer techniques were to be used for the measurement of electron density, collision frequency and recombination rates.

*Carried out under NASA Contract No. NAS 3-4103

IV. THEORETICAL ASPECTS

1. Optimum Seed Concentration In Ionized Gas by J. M. Smith and F. H. Shair

In the first quarterly report of this contract F. H. Shair considered the problem of maximizing the electrical conductivity of an ionized gas with respect to the seed concentration. In this analysis the electron temperature was assumed to be independent of the seed concentration and it was found that the optimum seed concentration increased with increasing degree of non-equilibrium. This conclusion was later discovered to be in contradiction to the results obtained in the diode experiments of reference (4) in which it was found that an approximately one order of magnitude decrease in the optimum seed concentration existed when the diode was operated in the non-equilibrium mode.

In this section the problem of maximizing the electrical conductivity with respect to the seed concentration is considered by including the dependency of the electron temperature on the seed concentration through the electron heating equation. This extension of the previous analysis leads to at least qualitative agreement with the results of reference (4).

We consider the following equations†:

$$\sigma = \frac{n_e e^2}{m\nu} \tag{1}$$

$$\nu = bQ_{es}(n_s - n_e) T_e^{1/2} + bQ_{en} n_n T_e^{1/2} + cn_e T_e^{-3/2} \ln\left(d\frac{T_e^3}{n_e}\right) \tag{2}$$

$$\frac{n_e^2}{n_s - n_e} = \chi(T_e) \tag{3}$$

$$\frac{T_e}{T} = 1 + \frac{1}{3}\gamma\omega^2\tau^2(1-K)^2 \mathcal{M}^2 \equiv 1 + \frac{f}{\nu^2} \tag{4}$$

where:

$$\begin{aligned} b &= 6.212 \times 10^5 \\ c &= 1.79 \\ d &= 1.5347 \times 10^8 \\ \chi &= 2.4147 \times 10^{15}\, T_e^{3/2} e^{-T_i/T_e} \end{aligned} \tag{5}$$

and it is assumed that the cross sections are constant.

Differentiating equation (1), (2), (3), (4), and (5) with respect to n_e we obtain

$$\frac{d\sigma}{dn_s} = \frac{e^2}{m\nu}\frac{dn_e}{dn_s} - \frac{n_e e^2}{m\nu^2}\frac{d\nu}{dn_s} \tag{6}$$

† Symbols are defined on page 23 .

$$\frac{d\nu}{dn_s} = bQ_{es}\left(1 - \frac{dn_e}{dn_s}\right)T_e^{1/2} + \frac{1}{2}\,\nu\,\frac{1}{T_e}\,\frac{dT_e}{dn_s} + cT_e^{-3/2}\ln\left(d\frac{T_e^3}{n_e}\right)\frac{dn_e}{dn_s}$$

$$- cn_eT_e^{-3/2}\ln\left(d\frac{T_e^3}{n_e}\right)\frac{1}{T_e}\,\frac{dT_e}{dn_s} + cn_eT_e^{-3/2}\left(3\frac{1}{T_e}\,\frac{dT_e}{dn_s} - \frac{1}{n_e}\,\frac{dn_e}{dn_s}\right) \tag{7}$$

$$\frac{dn_e}{dn_s} = \frac{\chi}{\sqrt{\chi^2 + 4n_s\chi}} - \frac{1}{2}\left[1 - \frac{\chi + 2n_s}{\sqrt{\chi^2 + 4n_s\chi}}\right]\frac{d\chi}{dT_e}\,\frac{dT_e}{dn_s} \tag{8}$$

$$\frac{dT_e}{dn_s} = -2T\frac{f}{\nu^3}\,\frac{d\nu}{dn_s} \tag{9}$$

$$\frac{d\chi}{dT_e} = \left(\frac{3}{2} + \frac{T_i}{T_e}\right)\frac{1}{T_e}\,\chi \tag{10}$$

The condition for optimum seed concentration is obtained from equation (6) by setting $d\sigma/dn_s = 0$. Equations (7) - (10) are then substituted into this condition to obtain, after considerable algebraic manipulation,

$$\frac{n_n}{n_s} \equiv \frac{1}{\alpha} = \frac{Q_{es}}{Q_{en}}\left\{\frac{-1 + \frac{2}{\beta}\left(-1 + \sqrt{1+\beta}\right)\sqrt{1+\beta} + 2\left(1 - \frac{T}{T_e}\right)\left(1 + \frac{T_i}{T_e}\right)\left[1 - \frac{2}{\beta}\left(-1 + \sqrt{1+\beta}\right)\right]}{2 - \frac{T}{T_e}}\right\}$$

$$+ \frac{c}{bQ_{en}T_e^2}\left[3\left(1 - \frac{T}{T_e}\right)\ln\left(d\frac{T_e^3}{n_e}\right) - 6\left(\frac{7}{6} - \frac{T}{T_e}\right)\right]\frac{\frac{2}{\beta}\left(-1 + \sqrt{1+\beta}\right)}{2 - \frac{T}{T_e}} \tag{11}$$

where $\beta = \dfrac{4n_s}{\chi}$

In the equilibrium case $T_e = T$ and slight degrees of ionization, i.e., $\beta >> 1$, we obtain

$$\frac{n_n}{n_s} \equiv \frac{1}{\alpha} = \frac{Q_{es}}{Q_{en}}$$

which is the common expression given for the seed concentration. In the non-equilibrium case, i.e., $T_e > T$, and for low degrees of ionization, $\beta >> 1$, we obtain

$$\frac{n_n}{n_s} = \frac{1}{\alpha} = \frac{Q_{es}}{Q_{en}} \left[\frac{1 + 2\left(1 - \frac{T}{T_e}\right)\left(1 + \frac{T_i}{T_e}\right)}{2 - \frac{T}{T_e}} \right]$$

or

$$\alpha = \frac{Q_{en}}{Q_{es}} \quad \frac{2 - \frac{T}{T_e}}{1 + 2\left(1 - \frac{T}{T_e}\right)\left(1 + \frac{T_i}{T_e}\right)}$$

which for $T_i >> T_e >> T$ yields

$$\alpha = \frac{Q_{en}}{Q_{es}} \; \frac{T_e}{T_i}$$

and since $\frac{T_i}{T_e} \simeq 10$ we see the order of magnitude decrease in X for the non-equilibrium case.

In Figure 5A α as given by equation 11 divided by Q_{en}/Q_{es}, i.e., ratio of non-equilibrium concentration to equilibrium concentration, is plotted as a function of electron temperature for various gas pressures and electron-Argon cross sections of 4.7×10^{-17} and 8×10^{-17} cm^2. It is noted that this ratio is relatively independent of gas pressure and assumption as to the magnitude of the electron-neutral cross section.

In Figure 5B the ratio of non-equilibrium to equilibrium concentration is plotted as a function of electron temperatures for various gas temperatures and electron-Argon cross sections of 4.7×10^{-17} and 8×10^{-17} cm^2. It is noted that for T_e slightly greater than T that the ratio is relatively independent of gas temperature and the magnitude of the cross section.

It is concluded from the above results that the ratio of non-equilibrium to equilibrium concentration is relatively independent of gas properties, relatively independent of cross section, and of order 10^{-1}. This is a relatively important result in that it shows that a MHD generator operating in the non-equilibrium mode will be operated optimally at lower seed concentration than the equilibrium generator which should greatly reduce the corrosion problem inherent with alkali metal atmospheres.

2. MGD Flows in a Recombining Plasma by J. M. Smith

During a pre-ionization experiment with the electron beam, a surprisingly slow decay in electron density was measured with the microwave interferometer. A one-dimensional analysis, developed under an AFOSR program*, was applied to the results. The main features of the analysis are given below.

For one-dimensional inviscid MHD flow, the equations are

continuity: $$\rho UA = \text{const} \tag{1}$$

momentum: $$\rho U \frac{dU}{dx} + \frac{dp}{dx} = (\overline{j} \times \overline{B})_x \tag{2}$$

energy: $$\rho U \frac{d}{dx} \left(C_p T + \frac{U^2}{2} = \overline{j} \cdot \overline{E} \right) \tag{3}$$

state: $$p = \rho RT \tag{4}$$

current:
$$j_x = \frac{\sigma}{1+\beta_e^2} \left[E_x - \beta (E_y - UB) \right] \tag{5}$$

$$j_y = \frac{\sigma}{1+\beta_e^2} \left[E_y - UB + \beta E_x \right] \tag{6}$$

Instead of the usual assumption σ = const., it is used in its defined form

$$\sigma = \frac{n_e e^2}{m\nu} \tag{7}$$

The equation for the electron density is given by the rate equation

$$\frac{d}{dx} \left[n_e U_e \right] = -n_e^3 \nu_{r_3} + n_e n_s \nu_{i_3} - n_e^2 \nu_{r_2} + n_p n_s \nu_{i_2} \tag{8}$$

where, on the right, the first two terms represent three body recombination and ionization and the last two terms represent two body recombination and ionization. The recombination rate coefficient ν_{r_3} was determined as a function of electron temperature from reference (6), and ν_{r_2} was estimated similarly from reference (7). In order that thermodynamic equilibrium can be achieved, the ionization rate coefficients, ν_i, were determined by the method of detailed balance so that equation (8) takes the form

*Contract No. AF 49(638)-1465

$$\frac{d}{dx} n_e U_e = - \left[1 - \frac{n_s - n_e}{n_e^2} \left(\frac{n_e^2}{n_s - n_e} \right)_{eq} \right] n_e^3 \nu_{r_3} \tag{9}$$

$$- \left[1 - \frac{n_s - n_e}{n_e^2} \left(\frac{n_e^2}{n_s - n_e} \right)_{eq} \right] n_e^2 \nu_{r_2}$$

$$\equiv \frac{d}{dx} n_e U_e \Big|_3 + \frac{d}{dx} n_e U_e \Big|_2$$

where

$$\left(\frac{n_e^2}{n_s - n_e} \right)_{eq} = \left(\frac{2\pi m k T_e}{h^2} \right)^{3/2} \exp \left(- \frac{e\phi_i}{kT_e} \right), \tag{10}$$

$$\nu_{r_3} = \frac{3.2 \times 10^{-10}}{T_e^5} \text{ for cesium} \tag{11}$$

$$\nu_{r_2} = \frac{1.44 \times 10^7}{T_e^{0.7}} \tag{12}$$

The electron temperature was determined from the electron energy equation

$$n_e U_e \frac{d}{dx} \left[5/2\, kT_e + \frac{mU_e^2}{2} \right] = \bar{j} \cdot \left[\bar{E} + \bar{U} \times \bar{B} \right] \tag{13}$$

$$- \sum_j n_e \nu_{ej} \left(2 \frac{m}{M_j} \right) 3/2\, k (T_e - T)$$

$$+ \left(\phi_i + 5/2\, kT_e + \frac{mU_e^2}{2} \right) \frac{d}{dx} n_e U_e \Big|_3$$

where in the last term the three body contribution only is included since radiation does not affect the electron energy. The collision frequencies ν_{e_i} are

$$\nu_{en} = n_a Q_{en} \left(\frac{8\, kT_e}{\pi m} \right)^{1/2} \tag{14}$$

$$\nu_{ei} = n_e \frac{16\pi}{3} \left(\frac{e^2}{m}\right)^2 \left(\frac{2kT_e}{m}\right)^{-3/2} \ln\left[3/2 \frac{1}{e^3} \left(\frac{K^3 T_e^{\ 3}}{\pi n_e}\right)^{1/2}\right] \qquad (15)$$

$$\nu_{es} = n_s Q_{es} \left(\frac{8\,kT_e}{\pi m}\right)^{1/2} \qquad (16)$$

The above set of equations are still indeterminate to the extent that the channel configuration, A (x), is under the control of the experimenter. For simplicity, A is chosen so that $U = U_o$ = constant and the analysis is further restricted to the segmented electrode case, i.e.

$$j_x = o, \; E_x = \beta\,(E_y - UB) \qquad (17)$$

$$j_y = \sigma\left[E_y - UB\right] \qquad (18)$$

Defining K through $E_y = K\,UB$ (19)

then $j_y = -\,\sigma\,(1-K)\,UB$ (20)

and $U_e = U_o$ (21)

The equations governing the flow then reduce to

$$\rho A = \rho_o A_o \qquad (22)$$

$$\frac{dp}{dx} = \bar{j} \times \bar{B} = -\,\sigma\,(1-K)\,U_o\,B^2 \qquad (23)$$

$$\rho U_o \frac{d}{dx} C_p T = -\,\sigma(1-K)\,KU_o^2\,B^2 \qquad (24)$$

$$p = \rho RT \qquad (25)$$

$$\sigma = \frac{n_e e^2}{m\nu} \qquad (26)$$

$$\frac{dn_e}{dx} = -\left[1 - \frac{n_s - n_e}{n_e^{\ 2}} \left(\frac{n_e^{\ 2}}{n_s - n_e}\right)_{eq.}\right]\left[\frac{n_e^3 \nu_{r_3}}{u_o} + \frac{n_e^2\,\nu_{r_2}}{u_o}\right] \qquad (27)$$

$$n_e U_o \frac{d}{dx} \frac{5}{2} kT_e = \sigma (1-K)^2 U_o^2 B^2 - \sum_j n_e \nu_{ej} \left(\frac{2m}{M_j}\right) 3/2\, k (T_e - T)$$

$$- \left(\phi_i + 5/2\, kT_e + \frac{mU_o^2}{2}\right) \frac{d}{dx} (n_e U_o) \Big|_3 \qquad (28)$$

Equations 23, 24, and 25 can be solved so that equation 24 can be replaced by

$$\frac{T}{T_o} = \left(\frac{p}{p_o}\right)^{\frac{K(\gamma-1)}{\gamma}} \qquad (29)$$

where

$$\gamma = C_p/C_v \qquad (30)$$

The seed density n_s is given through the seed fraction α by

$$n_s = \alpha\, n_a \qquad (31)$$

and $n_n \simeq \frac{p}{kT}$

In the electron beam experiments the magnetic field was zero between the beam port and the microwave station and therefore the above equations were integrated down the MHD channel with $B = 0$. The application of this analysis is described in Section VI.

V. EXPERIMENTAL APPARATUS

The bulk of the experimental apparatus remained the same as described previously (5), with the following being the principal changes effected for the present program, together with additional comments. A sketch of the complete facility is shown in figure 1.

1. Generator Channels

As previously reported, the subsonic channel had a constant 1 cm. x 3 cm. cross-section and was made of GE A976 dense aluminum oxide ("lucalox"). A second subsonic channel, used for obtaining the data in this report, was assembled in Dec. 1964 with several types of cathode (described below) and voltage profile measuring wires (0.625 mm diameter molybdenum) as shown in figure 2.

The supersonic lucalox channel for a Mach number $\mathcal{M}$ = 1.5 is shown in figure 3. The channel entrance is 2 cm. x 3 cm. and the shorter sides diverage in the flow direction to compensate for boundary layer growth. The details of the supersonic nozzle and channel design are given in Appendix I. The method of assembly was the same as for the subsonic channels, except that the layer of Resco AA22 potting cement, used as an insulating structural support, had to be thinner than before since the channel was twice as wide, and the pole face gap was held constant at 5 cm.

Lucalox has exhibited a high degree of resistance to surface attack from cesium seeding, the principal effect being a light brown discoloration which produced no detectable deterioration in the high electrical resistance required, and was almost completely removable when scrubbed in a detergent solution. A disadvantage in the use of lucalox is its rather poor thermal shock property, and this appears to limit the useful life of a subsonic section to 10-15 hours high temperature operation, the corresponding figure for the wider (higher wall temperature gradient) supersonic channel being 5-10 hours. A typical test in either channel required an hour of high temperature operation, and the life problem was probably aggravated by the inclusion of water-cooled test section side plates for magnet pole face protection. Initial hair line surface crazing in the lucalox progressively developed into definite breaks which allowed cold-trapping of cesium and subsequent attack of the potting compound between the lucalox and the side plates. The resulting products then entered the test section, contaminating the walls and the electrodes. This conclusion was drawn from the results of an X-ray diffraction analysis carried out on a sample taken from the supersonic channel and found to contain phosphorus, an element in the potting cement binder.

2. Electrode Materials

The following materials were used for electrodes:

1) molybdenum
2) 2% thoriated tungsten
3) barium oxide coated tungsten
4) barium strontium tungstates

$[Ba_5St(WO_6)_2 + 5\,BaO \cdot SrO \cdot 2WO_3]$ plus tungsten and a small amount of zirconium.

Under appropriately clean conditions, the last type as a cathode is capable of an emission of 12 A/cm^2 minimum at 1273°K in atmospheric pressure argon. Unfortunately, the method of weld mounting adopted and poisoning in the cesium-seeded argon prevented attainment of proper breakdown of the plasma under conditions where the first three types were operable.

A boron nitride mounted 200 watt tungsten lamp filament, intended for use as a directly heated cathode, was tested in an argon atmosphere to a temperature of 2100°K. A photograph of a complete cathode before insertion into the channel is shown in figure 4. Channel testing of this type of cathode was never realized because cesium attack of the sealants used produced too much contamination and necessitated channel disassembly and cleaning. Better success was obtained with an indirectly heated barium oxide cathode, but in this case, the maximum temperature attainable was a modest 1500°K at zero flow velocity and room temperature.

3. Cold Cathode Electron Beam

After adding a quadrupole magnetic focus system to the electron beam apparatus it was possible to pass a maximum safe current into the plasma of 0.1 ma at approximately 20,000 volts without danger of rupturing the aluminum foil window. This focusing system was capable of modulation at a low frequency (7 cycles/sec) for diagnostic purposes.

4. Recording System

Two 24 channel Minneapolis-Honeywell Visicorder high speed oscillographs with light sensitive recording paper were installed for the continuous monitoring of various quantities of interest such as electrical parameters associated with the generator channel and the output of strain gage pressure transducers. Temperatures were recorded, as before, on Electronik 17 recorders and a General Electric 24 Multipoint Recorder.

5. Cesium Seed Injection

This was improved by replacing the original fixed speed drive by a variable speed motor, the injection rate being determined from a gear tooth operated switch which caused a pulsed signal to appear on one channel of each Visicorder. In this way, it was also more convenient to relate timewise the two sets of records.

VI. EXPERIMENTAL PROGRAM AND RESULTS

1. The Electron Beam in the Subsonic Channel

Experimental measurements of electron density made by microwave interferometry were reported in reference 8 and are shown in Figures 6 and 7. Initially, measurements were made with the electron beam off in order to provide a reference for beam on measurements. The electron beam was injected through the Aluminum foil, and enhanced electron densities were measured 19 centimeters downstream from the beam port by the microwave interferometer for several neutral gas temperatures. The temperatures indicated in parenthesis are the electron temperatures corresponding to Saha equilibrium at the indicated electron density and gas conditions. However, the recombination analysis predicts that the actual electron temperature (see below) at the interferometer station will have fallen to a value near the neutral gas temperature. As a result, the calculated conductivities, using the indicated electron temperatures, are pessimistically low but are still 10-20 times the "beam off" value, as shown in Figure 7. These results generally confirm those of similar experiments reported in reference 5. Microwave attenuation experiments were attempted for determination of the collision frequency and thereby the electron temperature, but were unsuccessful due to inadequate resolution.

In the vicinity of the beam port gas conditions are now estimated to have been $p_{static} \cong 34$ psia, $u \cong 300$ m/sec ($M \cong 0.4$). Allowing for the reduction in static gas temperature below the total gas temperature due to the Mach number effect requires a shift in the temperature axis of 100°K, for the experimental points only, as compared to the figures reported in reference 8. Also, the conditions at the beam entry port were not noted in reference 8 but are shown now on Figures 6 and 7. It should be noted, however, that since the experimental conditions are estimated there is an uncertainty in the horizontal location of the experimental data points of perhaps $\pm 50^{\circ}$K.

Despite some experimental uncertainty two relatively definite conclusions can be drawn from these results. One, there seems to be some residual ionization in the plasma presumably frozen in during expansion in the nozzle to $M \cong 0.4$. Secondly, electron densities and conductivities more than an order of magnitude greater than those existing with the beam off wire observed when the beam was turned on. In conclusion, it must be noted that quantitative use of the above experimental results must be deferred until additional experiments are carried out under more carefully controlled conditions.

A simple theoretical model has been used to predict the conductivity at the beam injection port. It was assumed that electron-ion pairs were created uniformly throughout the plasma by mono-energetic electrons of energy E. It was further assumed that, on average, an energy of V_o ev was required to produce an electron-ion pair and that the volume within which the beam existed was swept out UA times per second. Then knowing the total beam current I entering the plasma, the electron density created was determined from $I = V_o \, UA \, n_e/E$. The electron temperature compatible with this value of n_e allowed determination of a corresponding conductivity. Using measured values of I, U, E andA and a conservative value of $V_o = 30$ ev for the cesium seed leads to a conductivity of 5 mho/m for $T_g = 1405^oK$ (a value shown in figure 8). Comparison of this value with the one inferred (4 mho/m at $n_e = 3.2 \times 10^{12}$ cm^{-3}) 19 cm downstream of the beam injection port suggested that a remarkably slow re-combination rate existed, even when allowing for a degree of inaccuracy in the simple model adopted for calculation of the initial conductivity.

Application of the theoretical recombination analysis of Section IV.2 to the experimentals points obtained is shown in Figures 8A, 8B, 8C

In order to correlate the data various values of n_e at the electron beam port were chosen until the value of n_e at the microwave port agreed with experiment. The value of T_e at the electron beam port was chosen to satisfy Saha's equation at the assumed initial electron density. It was found that the electron temperature fell to approximately the gas temperature in the order of a cm (see Fig. 8A) while the electron density decayed very slowly and remained well above the value it would have in Saha equilibrium with the electron temperature (see Figs. 8B and 8C).

The above calculations were carried out for the highest ($3.2 \times 10^{12} \frac{\text{electron}}{\text{cm}^3}$) and the lowest ($12 \times 10^{12} \frac{\text{electron}}{\text{cm}^3}$) electron densities measured at the microwave port. From the initial values of electron density necessary to obtain these values the energy to produce an electron-ion pair was calculated. This value varied from 14.2 to 86.7 ev and this range includes the average value of 32 ev which is generally assumed for electron-ion pair production. It was therefore concluded that the theory at least qualitatively explained these preliminary experimental points; i.e., the electron density was partially frozen.

2. Non-Equilibrium Ionization in Subsonic Flow

Before conducting power generation experiments, tests were performed with applied electric fields on one pair of electrodes in the subsonic channel in the presence of a magnetic field. Data was recorded for both directions of the applied electric field using the circuit of figure 9 in which voltage and current were recorded by galvanometers. The resulting electrode voltages and currents are plotted in figure 10. It appears that there was a sheath voltage at which appreciable current started flowing smoothly, the difference in voltage between the two curves at constant current being attributed to twice the net induced voltage V_g. Thus for an approximately constant difference of 5 volts, V_g = 2.5 volts, representing 8.7% of the theoretical value of UBl = 28.8 volts for the conditions of the experiment. Furthermore, the zero current sheath voltage was approximately 17 volts. If this sheath voltage is assumed constant with current and is subtracted, the resulting conductivities were of the order of σ = 100 mho/m, and since only one electrode pair was being used, the scalar conductivities in the channel were very high. Two typical single frames from a cine camera record of the discharge are shown in figure 11; throughout the current range when the discharge was visible it had a uniform diffuse appearance with no evidence of streamers or arcs.

The results of an applied voltage experiment with a magnetic field of 24,000 gauss and using a metastable (Penning) mixture of mercury and cesium are shown in figure 12. The curve for which the induced and applied electric fields are additive (2% thoriated tungsten cathode) is closely similarly to the corresponding curve of figure 10 except that the initial voltage for appreciable current flow was approximately 65% higher with the Penning mixture. This was followed by a rapid decrease in voltage with increasing current until similarity of the two curves resulted and then both current and voltage increased together. Similar remarks apply to the case where the induced electric field subtracted from the applied electric field (unheated BaO cathode), but the initial voltage for current flow was even higher (approximately 120%) and the final similarity with the corresponding curve of figure 10 was not as close as for the additive electric field case. Furthermore, for currents greater than 0.6 amp, the average net induced voltage was approximately the same as with cesium seeding (figure 10). Thus, compared with cesium seed, the Penning mixture inhibits the initial flow of current to a certain breakdown point after which the voltage-current characteristics are fairly similar. On this basis, cesium seeding appears preferable except that, with the Penning mixture, the breakdown point may correspond to the onset of extensive volumetric photo-ionization along the channel instead of just local ionization between the electrodes. In reference 5, microwave interferometer measurements upstream of the electrodes during a similar experiment indicated the occurrence of such a phenomenon.

The results of applied voltage experiments without magnetic field for different electrode materials using cesium and mercury seed are shown in figure 13. It is seen that on decreasing the voltage a higher current is passed compared with that for the same ascending voltage, presumably due to better cathode emission as a result of temperature rise after a period (~ 10 sec) of ionic bombardment. In addition, the performance of a barium oxide coated cathode is superior to that of a 2% thoriated tungsten cathode with respect to emission and zero current sheath voltage. With cesium seeding, the molybdenum cathodes are intermediate in performance which was essentially unaffected by an order of magnitude variation in seed rate. These latter results were obtained during subsonic checking of the supersonic channel as described in the next sub-section, and were not accompanied by the visual observation of a glow discharge. This fact was supported by the increased unsteadiness of the signal traces from which average values were obtained for the points plotted.

3. Use of the Supersonic Channel by N. A. Evans

The subsonic experiments indicated that appreciable electrode losses were present and that a higher induced voltage would be required for generating power. It was therefore decided to proceed directly to the supersonic channel which was theoretically capable of producing a value of UBl = 61 volts for B = 2.5 webers/m^2, $\mathcal{M}$ = 1.5 at T_o = 1500°K and l = 0.03 m.

On a preliminary test, related measurements of static and total pressure showed that the channel exit centerline Mach number was 1.80, the increase over the design Mach number of 1.50 being attributed to over-correction for viscous effects when using a friction factor f = 0.003. During this run the mass flow was 185 grm/sec at a maximum temperature of 1080°K which occurred as a result of resistance mis-match of the main heater element with its power supply. Since the stream static temperature was very low ($\sim$ 550°K on average along the channel) subsequent tests were conducted subsonicly in the supersonic channel at lower mass flows ($\sim$ 80 gms/sec) in order to achieve higher static temperatures in the range 1200 to 1400°K while the establishment of a glow discharge from d.c. pre-ionization was being checked out. After completing this stage, it was intended to give a rapid increase in mass flow to achieve supersonic operation for a short period ($\sim$15 sec) at high temperature by making use of the small thermal capacity of the main heater. This objective was never realized on account of difficulty in achieving the desired pre-ionization glow discharge. Main heater failure (after 42 successful cycles to high temperature) was followed by several almost consecutive failures of a new element and one severe case of channel and electrode contamination when the directly heated cathode sealants decomposed. In addition, the section immediately downstream of the seed injection station was severely attacked by cesium. A photograph of the seeding station and the adjacent downstream section is shown in figure 14, and it can be seen that the cesium was not vaporizing efficiently. The decomposed molded alumina section was replaced by one of boron nitride, the seed spray bar was modified and the directly heated cathodes were replaced by plain molybdenum types.

When the channel was dismantled on a second occasion for cleaning, breaks were found in the lucalox walls, and it was apparent from X-ray diffraction analysis that the products of cesium attack on the potting cement behind the lucalox were contributing to the contamination problem. The subsonic section was then re-installed while the system was being further checked out, and during this time it became evident that the succession of new heater elements was introducing an insulative contamination by the sublimation into the hot argon stream of an oxide from the surface of the molybdenum wire mesh: a wall deposit downstream of the heater exit was found to be rich in an oxygen deficient molybdenum oxide when subjected to analysis.

The heater failure problem was finally solved by making a tightly rolled element with as much molybdenum wire mesh as could be fitted into the ceramic tube housing, and by installing a second transformer to provide proper matching with the power supply. After an initial shakedown cleaning run, satisfactory glow discharges for 10-15 second periods were obtained in the cleaned subsonic channel only when seed injection (at $X_{Cs} \sim 1\%$) was stopped. Apart from visual observation, the oscillograph records showed precisely that the nature of the discharge changed when seed injection was switched on and off. It was apparent that incomplete seed vaporization was still occurring, but it is not clear why the glow discharge was extinguished with seed injection. These glow discharge results have not been reported because the effective seed rate was uncertain and varying with time. This test was the last that could be conducted during the contract period covered by this report, and the interpretable results obtained have been included in the previous sub-section, since they were recorded during subsonic operation of the supersonic channel.

VII. CONCLUSIONS

A theoretical investigation of the seed concentration to produce an optimal electrical conductivity in a magnetically induced non-equilibrium MHD generator showed that the concentration could be reduced by the factor

$$\frac{2 - \frac{T}{T_e}}{1 + 2\left(1 - \frac{T}{T_e}\right)\left(1 + \frac{T_i}{T_e}\right)}$$

approximately. From the above expression it is seen that when appreciable non-equilibrium exists, i.e., $T_i \gg T_e \gg T$, that the concentration is reduced by $T_i/T_e \simeq 10$. This represents a significant reduction in the alkali metal seed concentration requirements and hence should significantly reduce contamination and corrosion problems which have appeared to plague the performance of alkali metal seeded MHD generators.

The experiments with the electron beam as a pre-ionizing agent in the subsonic channel have shown that significant levels of non-thermal ionization are obtainable. Furthermore, measurements with the microwave interferometer indicated a remarkable persistence along the channel of an elevated electron density, possibly due to the electron density itself being relatively low. However, on making reasonable assumptions concerning the magnitude of some of the physical parameters involved (such as the electron-ion pair production energy), good agreement between experiment and recombination theory has been demonstrated for at least the qualitative trends.

The effectiveness of the electron beam in a space power package application may be judged from the extent by which its use decreases the overall efficiency of the generator (8). Although in the present experimental situation only 0.1 mA out of a possible 50 mA available typically entered the channel (at 17,000 volts) on account of practical considerations, it appears reasonable at this stage to assume that a beam system with power supply could be designed with a power efficiency of 80%. In this case no foil window with its attendant losses would be required since a space vacuum would be available for differential pumping. It is also assumed that a sufficiently precise magnetic sheet focussing system would ensure that the total 0.1 mA beam current produced would go into the generator at its entrance with no losses suffered through recombination. Hence the required beam power would be $P_b = \frac{1700 \times 0.1 \times 10^{-3}}{0.8} = 2.1$ watts. An idealised estimate (neglecting sheath losses) of the generator power output for the conditions of the present experiment may be obtained from

$$P_g = - \sigma (1-K) K U^2 B^2 AL$$

where the load factor will be taken as K - 0.8 with σ = 3 mho/m calculated at the beam port (Section VI.1), U ≅ 470 m/sec, M ≅ 0.7, B = 5 webers/m^2, A = 3 x 10^{-4} m^2 and the generator length L = 0.2 m. Thus P_g ≃ 150 watts, and on this approximate basis, the generator power efficiency loss would be less than 2%, suggesting that electron beam pre-ionization has promising potential.

Experiments in the subsonic channel with applied electric and magnetic fields showd that the net induced voltage level was only a small fraction (8.7%) of the theoretically attainable, due presumably to the existence of large electrodes losses when apparently current was flowing. This occurred even though there was a good conduction path between electrodes during the presence of a glow discharge. The use of a cesium-mercury Penning seed mixture probably produced significant volumetric ionization but the zero current sheath voltage was appreciably higher compared with the pure cesium case.

Shock tube studies of actual power generation in the same laboratory (9) have conclusively indicated that significant short duration power is extractable when a sufficiently high induced voltage is produced to overcome the sheath losses. However, before attempting to generate voltages in a supersonic channel, further subsonic experiments with differect electrodes and seed materials suggested that barium oxide cathodes were far superior to 2% thoriated tungsten types, with plain molybdenum a fairly acceptable possibility. The influence of cathode deating from ionic bombardment appears to be definitely beneficial, but preliminary results indicated (for a molybdenum cathode) that performance was relatively unaffected by quite a large variation in seed concentration.

Supersonic experiments were hampered by a succession of equipment and materials problems which produced serious channel and electrode contamination with the unfortunate result that very little useful data were obtained.

VIII. FUTURE WORK AND RECOMMENDATIONS by N. A. Evans

The present study has emphasized the need for gaining a better basic understanding of electrical discharge phenomena in viscous seeded gas flows, and it is intended to continue experimental work from this point of view, paying particular attention to materials selection, channel design and the exclusion, as far as possible, of contaminating influences. Although dense aluminum oxide (lucalox) has shown a satisfactory resistance to alkali metal seed attack, it is rather susceptible to thermal shock and there are difficulties in producing gas tight seals. Boron nitride is definitely superior on the last two points, and appears capable of satisfactory performance in a low partial pressure seed environment if handled with care (1). Accordingly a boron nitride test section is presently under construction: external wall heating (instead of cooling) will be incorporated together with a high degree flexibility in the changing of electrode materials and geometry. In addition, the sections immediately upstream and downstream of the boron nitride channel will be independently heated to minimize the build-up of seed concentration at the walls which could lead to troublesome short-circuiting. Instead of a liquid spray, cesium seed will be injected as a vapor.

Initial experiments, using applied electric fields, will be concerned with the measurement, by positionable probes in the discharge region, of positive column fields and sheath voltages through a velocity range from essentially zero (static diode case) into the low supersonic regime; subsequent experiments will involve the use of an applied magnetic field. Microwave interferometer measurements will be used for determining electron densities, collision frequencies and recombination rates. In this way, it is hoped that a systematic picture can be built up of the nature of electrical discharge phenomena in seeded gas flows, and that some of the problems associated with continuous power generation involving non-equilibrium ionization can be elucidated.

IX. TABLE OF SYMBOLS

A	area
B	magnetic field strength
c_p	gas specific heat at constant pressure
C_τ	friction coefficient
E	electric field strength
e	electronic charge
I	current
j	current density
K	load factor = E_y/UB
k	Boltzmann constant
L	generator length
l	channel dimension normal to magnetic field
$\mathcal{M}$	Mach number
M	heavy particle mass
m	light particle mass
n	number density
P	power
p	pressure
Q	cross-section
R	gas constant
r_h	hydraulic radius = $\frac{2 \text{ area}}{\text{wetted perimeter}}$

T	temperature
U	velocity
V	voltage
X	molar seed fraction
x	coordinate in flow direction
y	coordinate transverse to flow direction
α	recombination coefficient
β	$\omega \tau$ or $4 n_s/x$
γ	ratio of gas specific heats
η	efficiency
θ	flow deflection angle
μ	viscosity, Mach angle
ν	collision frequency, recombination rate, or Prandtl-Meyer function
ρ	density
σ	conductivity
τ	collision time
ϕ	ionization energy
χ	temperature dependent function
ω	cyclotron frequency

Superscripts

*	condition related to $\mathcal{M} = 1$

Subscripts

0	constant value, stagnation value, output or source

2	2-body process
3	3-body process
d	design condition
av	average value
e	electron
eq	equilibrium
g	generated
i	ion, ionization or input
n	neutral particle
p	photon or plasma
r	recombination, radial distance from apparent source
s	seed
x	axial component
y	transverse component
Cs	cesium
Hg	mercury

X. BIBLIOGRAPHY

1. Cool, T. A. and Zukoski, E. E., "Recombination Rates and Non-equilibrium Electrical Conductivity in a Seeded Plasma." 6th Symposium on Engineering Aspects of MHD, Pittsburgh, Penna. 1965.

2. Sheindlin, A., Batenin, V. and Asinovsky, E., "Experimental Investigation of Non-equilibrium Ionization in a Mixture of Potassium and Argon." International Symposium on MHD Power Generation, Paris, 1964.

3. Golubev, V. S., Kasabov, G. A. and Kanakh, V. F., "Study of a Steady-State Argon-Cesium Plasma with Non-equilibrium Conductivity," Teplofizika Vysokikh Temperatur, Vol. 2, No. 4.

4. Ellington, H. I., "Low Voltage Diffuse Discharge in Atmospheric Pressure Helium and Argon Seeded with Small Amounts of Cesium, Potassium and Sodium," AERE-M1616, July 1965.

5. Shair, F. H., "Investigation of an MGD Power Generation Duct," NASA CR-54124, January 1965.

6. Dugan, J. V., "Three-body Collisional Recombination of Cesium Seed Ions and Electrons in High Density Plasmas with Argon Carrier Gas." NASA TN D-2004.

7. Bates, D. R., Atomic and Molecular Processes. Academic Press, New York, p. 252, 1962.

8. Shair, F. H. and Sherman, A., "Electron Beam Preionization in an MHD Generator," 6th Symposium on Eng. Aspects of MHD, Pittsburgh, 1965.

9. Zauderer, B., Effects Governing Magnetically Induced Ionization. Proc. Int. Symposium on MHD Electrical Power Generation, Vol. 4, Paris, 1964.

10. Crown, J. C., "Supersonic Nozzle Design," NACA TN 1651, June 1948.

11. Foa, J. V., "Elements of Flight Propulsion," John Wiley and Sons, Inc., New York.

12. Ruptash, J., "Supersonic Wind Tunnel - Theory, Design and Performance," UTIA Review #5, June 1952.

13. Handbook of Supersonic Aerodynamics, NAVORD Report #1488, Vol. 2.

14. Persh, J. and Lee, R. E., "A Method for Calculating Turbulent Boundary Layer Development in Supersonic and Hypersonic Nozzles, including the Effect of Heat Transfer," NAVORD Report $4200, June 1956.

15. Shapiro, A. H., "The Dynamics and Thermodynamics of Compressible Fluid Flow," Volumes I and II. The Ronald Press Company, New York.

16. Schlichting, H., "Boundary Layer Theory," McGraw Hill Book Company, Inc., New York.

XI. APPENDIX

Supersonic Channel Design

by

R. Chin

In a supersonic $\mathcal{M} = 1.5$, MGD channel operating at $T_o = 1500^{\circ}K$ with a channel height of 3 cm., the Hartmann number, which expresses the ratio of magnetic to viscous forces, is of the order one for a typical gas conductivity of 1 mho/m. It is not clear from past experience whether enough power can be generated to produce a Lorentz body force of sufficient strength to affect seriously the following design calculations. In view of this uncertainty, it has, for the present, been entirely neglected. The design, however, incorporates compensation for viscous effects only. Thus the MGD channel resembles a conventional supersonic wind tunnel for which the design procedure is well established.

The total channel length consists of a nozzle, a constant Mach number section with two divergent walls to correct for the viscous effects, and a diffuser where a fraction of the total pressure is recovered (figure 15a).

In the nozzle, Foelsch's (10) analytic method was employed and the calculation was particularly simple. It consisted of constructing a suitable contour to convert a radial supersonic flow into a uniform parallel one through wave cancellation at the wall past the inflection point. A third order polynomial was used for the initial part of the contour up to the inflection point, and it was assumed that a radial flow existed in this region.

The viscous channel calculations were performed by the method of influence coefficients (11) in a one-dimensional supersonic flow. This technique involves the viscous effect in terms of a section-averaged friction coefficient and the hydraulic radius of the cross-section.

Pressure recovery was assumed to be accomplished by a normal shock standing at the entrance to the diffuser and followed by a 6° divergent subsonic diffuser.

In the ensuring calculations, the following assumptions were made:

1) perfect gas with $\gamma = 5/3$
2) one-dimensional, adiabatic flow
3) $\bar{J} \times \bar{B}$ body force neglected
4) the exit pressure, $p_e = 1$ atm.
5) $T_o = 1500^{\circ}K$
6) standing normal shock at the entrance to the diffuser.

In addition, the design had to satisfy the following requirements:

1) the generator channel length was to be 40 cm. with an entry cross section of 2 cm. x 3 cm.,
2) an estimated maximum argon mass flow rate from the heater of 0.3 lb./sec. at $T_0 = 1500^\circ K$,
3) the electron beam equipment and microwave horns were to incorporate into the system.

A detailed analysis of the methods employed is as follows. For the nozzle, A is the wall inflection point as shown in figure 15b. Foelsch assumed a radial flow to exist there, so that AO, the arc of a circle of radius r_A around the apparent source, is an equipotential line along which the Mach number is constant. Thus,

$$\theta_A = AO/r_A$$

It can be shown by the method of characteristics that

$$\theta_A \leq \frac{\nu_D(\mathcal{M}_D)}{2}$$

For a given Mach number, the smaller the expansion angle θ_A (to a certain limit, see below) the less critical is the contour design in producing a uniform velocity in the test section. On the other hand, a smaller expansion angle results in a longer nozzle length and an increased boundary layer growth. It is suggested (12) that

$$\frac{1}{4}\nu_D < \theta_A < \frac{1}{3}\nu_D$$

From references 10, the terminal length $x_D - x_A$ is given by

$$\frac{x_D - x_A}{y_D} = \sqrt{\mathcal{M}_D^2 - 1} + \frac{1}{\theta_A}\left[1 - \frac{A_{A/A*}}{A_{D/A*}}\cos\theta_A\right] \qquad (1)$$

and

$$\frac{x_A}{y_D} = \frac{\mathcal{M}_D}{\frac{A_D}{A*}\tan\theta_A}\left[\frac{A_A}{A*}\,\frac{(57.3)\sin\theta_A}{\theta_A} - 1\right] \qquad (2)$$

Combining (1) and (2),

$$\frac{x_D}{y_D} = \sqrt{\mathcal{M}_D^2 - 1} + \frac{1}{\theta_A} \left[1 - \frac{A_{A/A*}}{A_{D/A*}} \cos \theta_A \right]$$

$$+ \frac{\mathcal{M}_D}{\frac{A_D}{A} \tan \theta_A} \left[\frac{A_A}{A*} \quad \frac{(57.3) \sin \theta_A}{\theta_A} - 1 \right] \qquad (3)$$

where A_N is the section area at any point N and A* is the throat area.

Thus, for any design Mach number, one can see that the length of the nozzle, x_D, depends upon θ_A. Foelsch chose a cubic for the initial supersonic portion since it satisfies the boundary conditions imposed on this part of the contour. However, the use of such an analytical curve does not ensure radial flow at the inflection point, but in practice, the resultant flow is generally satisfactorily close to design.

Therefore, for $y* \leq y \leq y_A$

$$\frac{y}{y*} = 1 \frac{x_A}{y*} \tan \theta_A \left(\frac{x}{x_A} \right)^2 \left[1 - \frac{1}{3} \left(\frac{x}{x_A} \right) \right] \qquad (4)$$

Integrating along the characteristic in the region ADE,

$$\frac{x}{y*} = \frac{r}{y*} \left[\cos \theta + \frac{(\theta_A - \theta) \cos (\theta + \mu)}{\sin \mu} \right] \qquad (5a)$$

and

$$\frac{y}{y*} = \frac{r}{y*} \left[\sin \theta + \frac{(\theta_A - \theta) \sin (\theta + \mu)}{\sin \mu} \right] \qquad (5b)$$

Furthermore,

$$\frac{r}{y*} = \frac{r}{r*} \quad \frac{r*}{y*} = \left(\frac{r}{r*} \right) \frac{1}{\sin \theta_A} \qquad (6a)$$

with

$$\frac{r}{r*} = \frac{1}{\mathcal{M}} \left[\frac{2 \left(1 + \frac{\gamma - 1}{2} \mathcal{M}^2 \right)}{\gamma + 1} \right]^{\frac{\gamma + 1}{2(\gamma - 1)}} \qquad (6b)$$

In addition, the Mach number distribution along A-D can be calculated by realizing that

$$\nu - \theta = \text{constant} = \nu_D \tag{7}$$

since $\theta_D = 0$.

Thus, the computation procedure may be summarized as follows:

1) For a given design $\mathcal{M}$, A_D/A^* can be obtained from standard compressible flow tables (12).

2) Chose a θ_A for $1/4\ \nu_d < \theta_A < \frac{1}{3}\nu_d$

3) Select a series of values for θ, $0 \leq \theta \leq \theta_A$ and apply equations (5), (6), and (7).

4) As a check, compute the terminal length from equation (3) and compare with the result obtained in steps (2) and (3).

A rough estimate of the boundary layer development (14) along the nozzle walls showed that δ_{D^*}/y_D was of the order of 10^{-3} for a boundary layer thickness assumed to be zero at the throat. Thus, the viscous effect in the nozzle section was neglected.

On the contrary, the channel design must be corrected for the viscous effect, e.g., Shapiro (15) gives a maximum length-diameter ratio of 14 before choking for an initial Mach number of 1.5 in a constant area duct with a friction factor f = 0.0025. The frictional effect is computed in terms of an average friction coefficient over a section length and the hydraulic radius of the cross-section.

Neglecting the $\bar{J} \times \bar{B}$ force and considering one dimensional, perfect gas flow, one can write the axial Mach number distribution as,

$$\frac{d\mathcal{M}}{\mathcal{M}} = \frac{1 + \frac{\gamma-1}{2}\mathcal{M}^2}{1 - \mathcal{M}^2}\frac{dA}{A} + \frac{\gamma\mathcal{M}^2\left(1 + \frac{\gamma-1}{2}\right)\mathcal{M}^2}{1 - \mathcal{M}^2}\frac{C_\tau}{r_h}d_x \tag{8}$$

For a constant Mach number channel ($d\mathcal{M} = 0$), with a rectangular cross-section of constant width w and a variable height ℓ, one obtains,

$$\frac{d\ell}{\ell + w} = \gamma\mathcal{M}^2\frac{C_\tau}{w}dx$$

On integrating

$$\ln(\ell + w) = \frac{\gamma \mathcal{M}^2}{w} C_\tau \, x \qquad (9)$$

Furthermore, the static pressure distribution is

$$p \, \ell = \text{constant}$$

Similarily, the stagnation pressure is also related to the channel shape as

$$p_o \ell = \text{constant}$$

for a constant axial Mach number.

In addition, it can be shown that the static temperature and the flow velocity along the flow direction are constant.

To complete the calculation, one needs to know C_τ, the average friction coefficient. It is suggested by Schlichting (16) that no appreciable difference exists in friction factor for a fully developed subsonic and supersonic flows.

A measurement of the representative friction factor was performed on the existing subsonic channel with a cross-section of 1 cm. x 3 cm. It was found to be .0067 approximately. Moreover, the flow was constricted by numerous voltage measuring pins which traverse the channel width. Attributing 50% of the pressure drop to these protruding wires, and scaling for the difference in hydraulic radius of the cross-section of the two channels, produced a friction coefficient of 0.003. This approximate value was used throughout the calculation.

Incorporating the listed restrictions into the above calculation methods produced the following final design:

1) the transition length (connecting the exit of the nozzle to the entrance of the test section) was 40 cm.

2) the mass flow rate at a stagnation temperature of 1500°K was approximately .30 lb./sec.

3) the channel wall shape was

$$\ell = 4 \, e^{.5625 \times 10^{-2} x} \quad -2$$

where x is measured from the exit of the nozzle.

4) the nozzle shape is shown in the table of figure 15b.

XII. ACKNOWLEDGMENT

Mr. A. Ruess gave valuable assistance by obtaining and reducing the microwave interferometer data.

The part played by Mr. G. Crolius and his staff of the machine shop is gratefully acknowledged.

Thanks are due to Mr. T. Shust and Mr. S. F. D'Abbene for their essential help during the preparation and the running of the experiments.

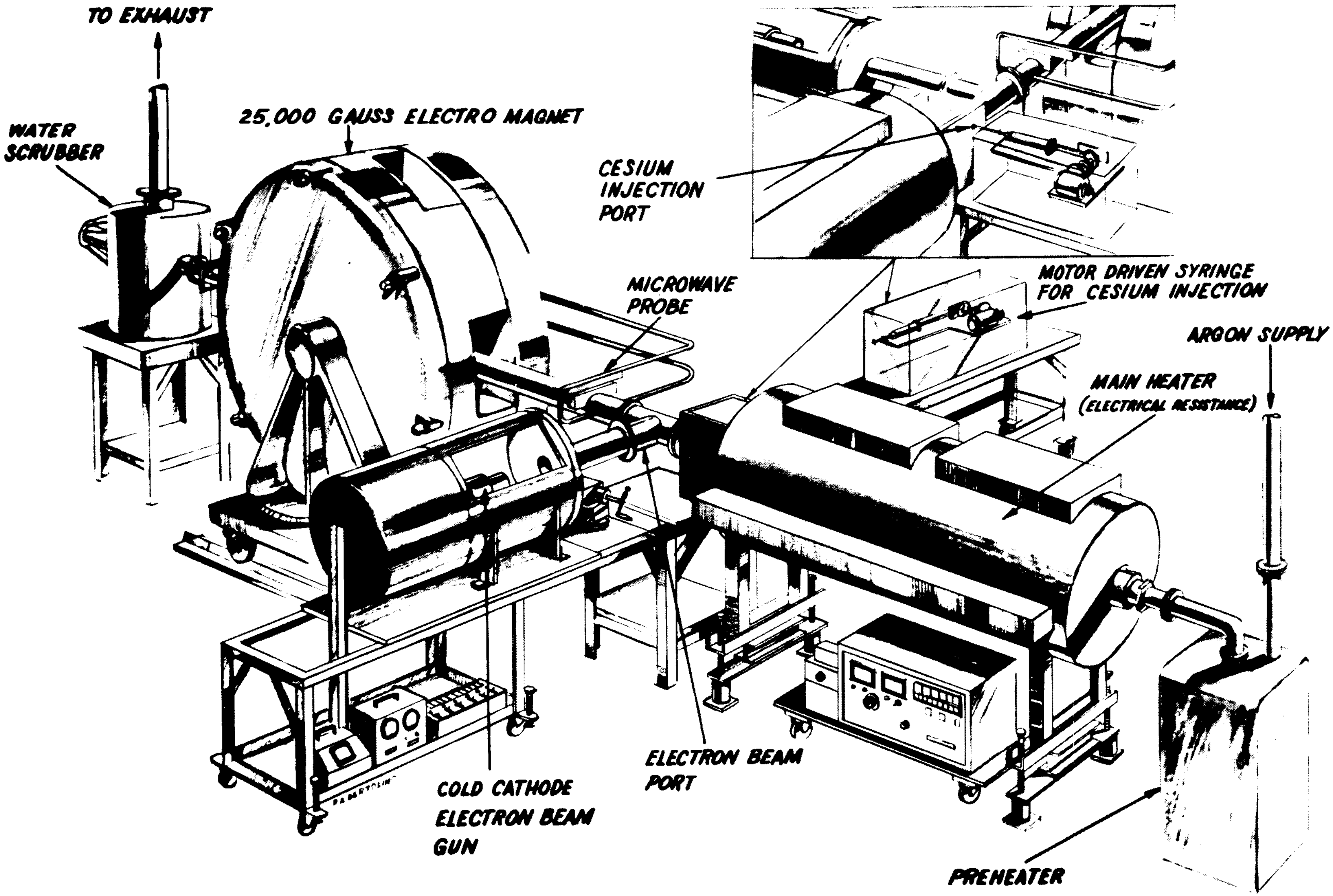

Figure 1. Seeded Gas MGD Facility

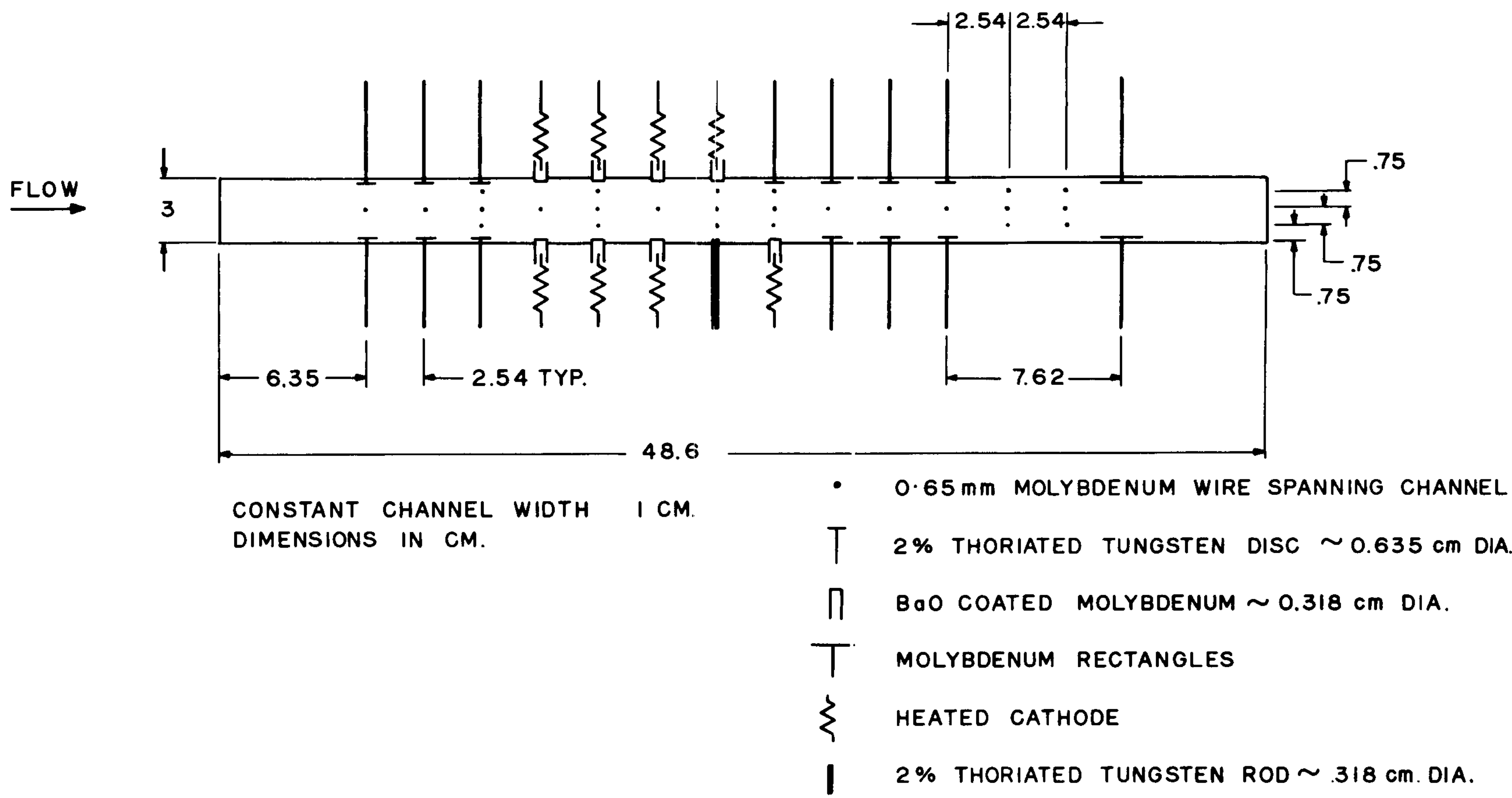

Figure 2. Subsonic Generator Channel Electrode Layout

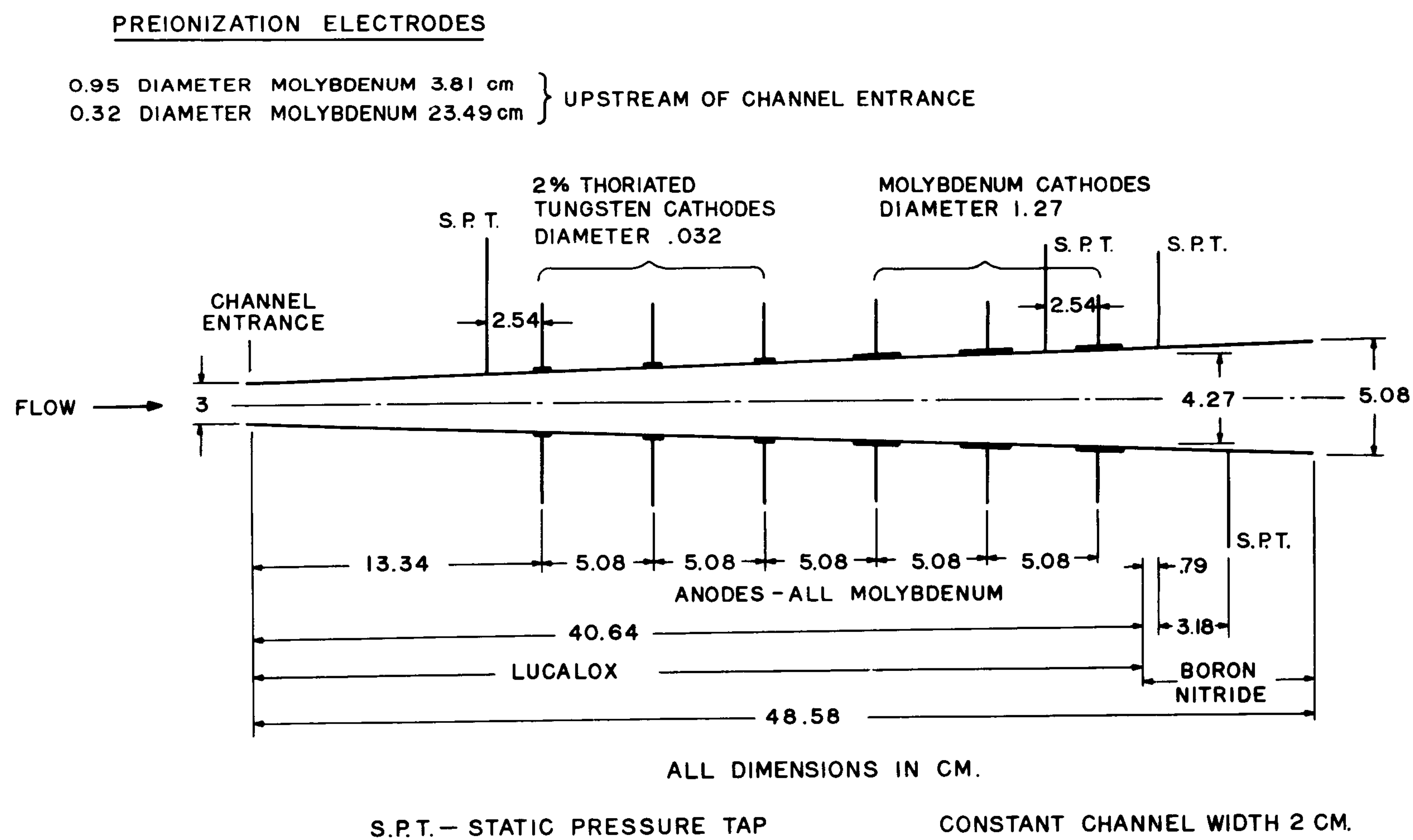

Figure 3. Supersonic Generator Channel (M=1.5) - Electrode Layout

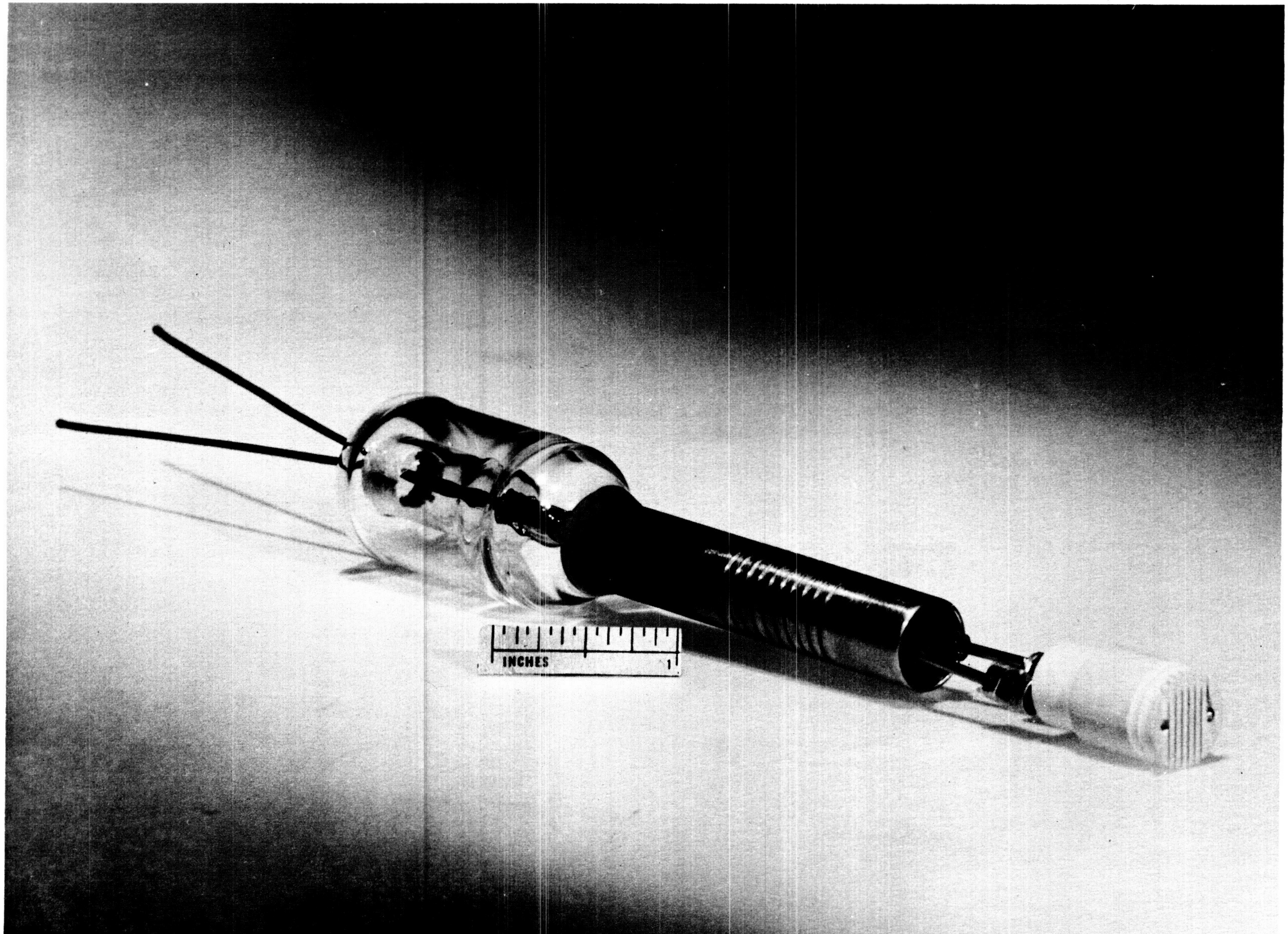

Figure 4. Directly Heated Tungsten Cathode

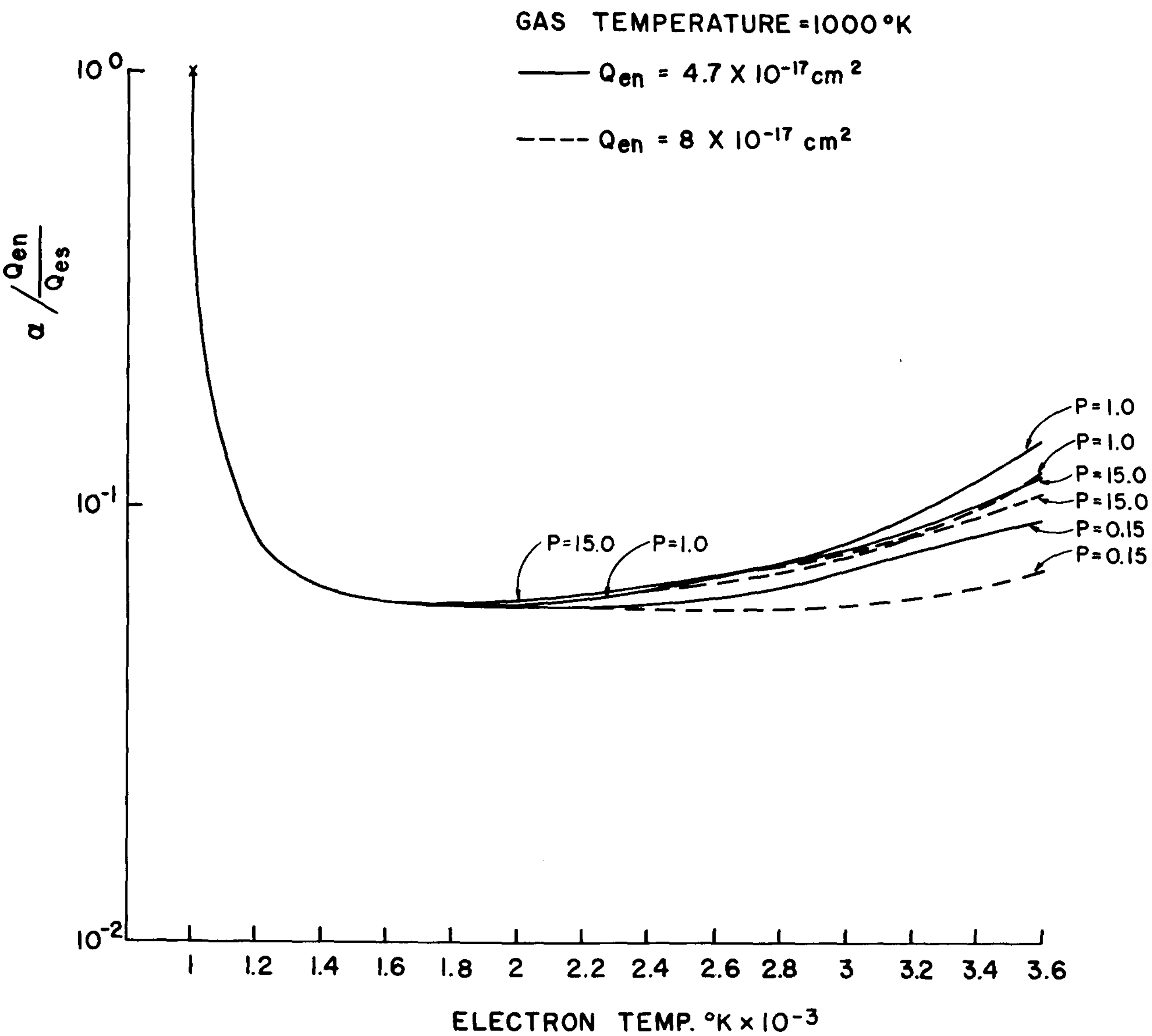

Figure 5A. Ratio of Non-equilibrium to Equilibrium Seed Concentration Vs. Electron Temperature As Function of Gas Pressure.

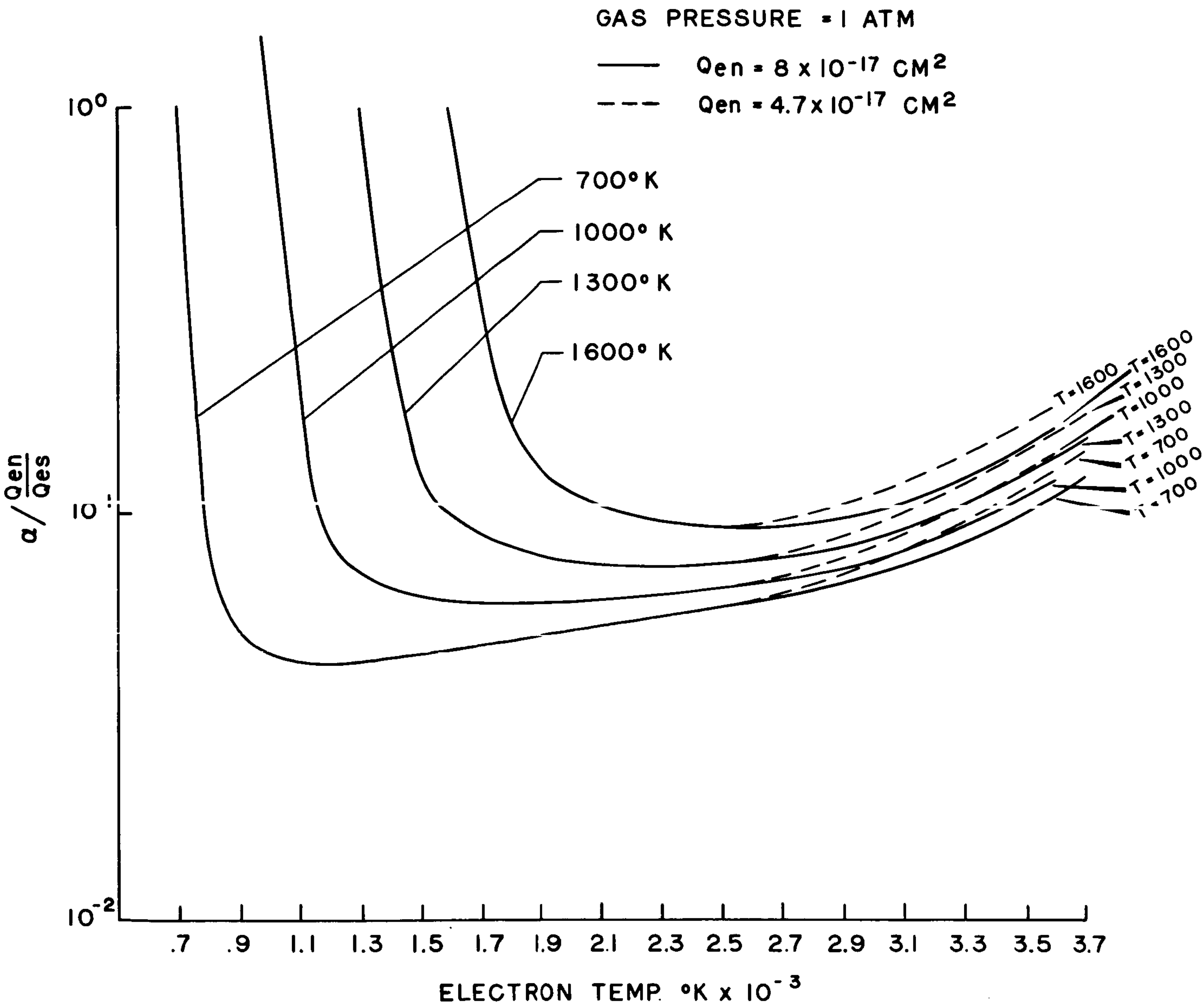

Figure 5B. Ratio of Non-equilibrium to Equilibrium Seed Concentration vs. Electron Temperature As Function of Gas Temperature

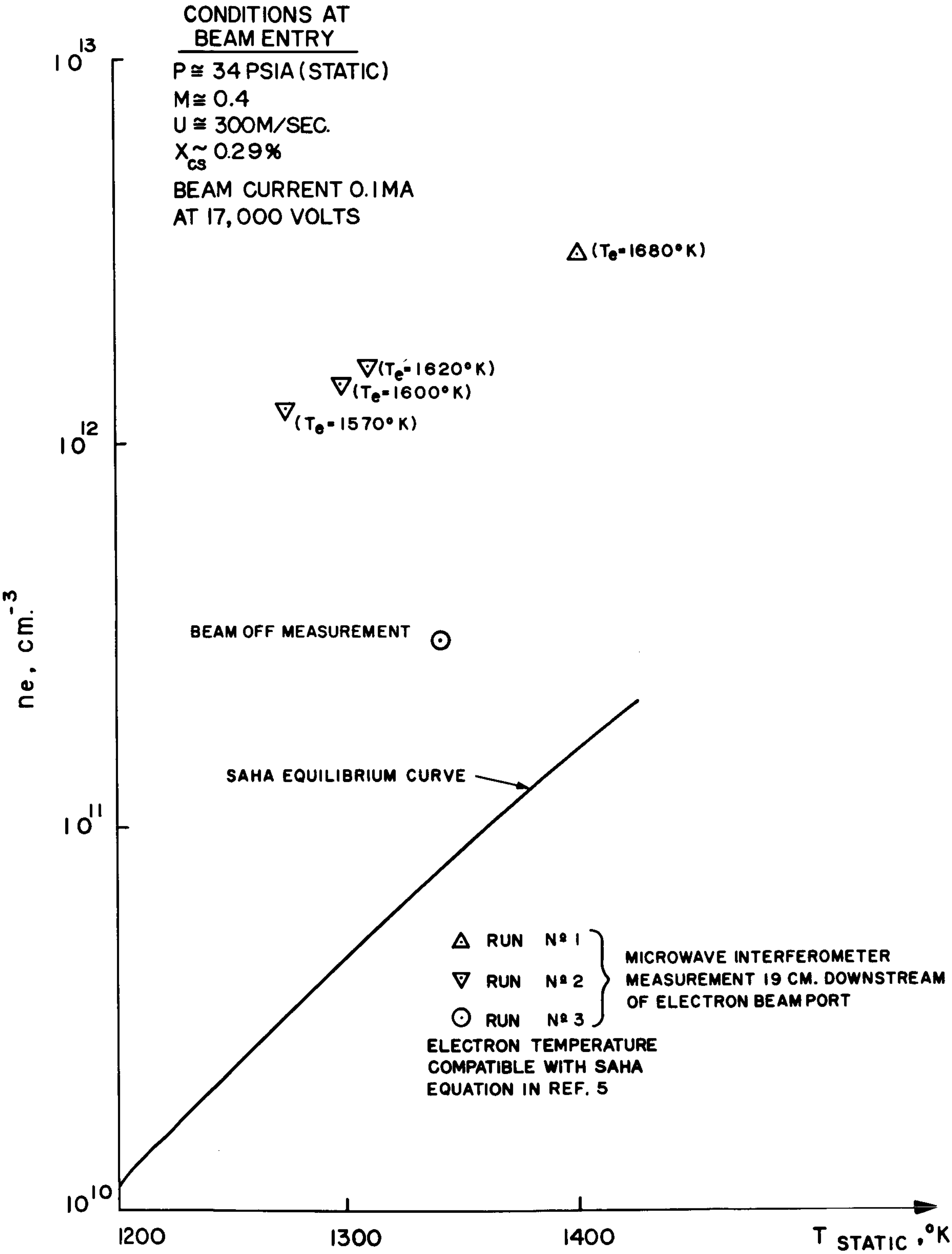

Figure 6. Electron Beam Enhancement of Electron Density

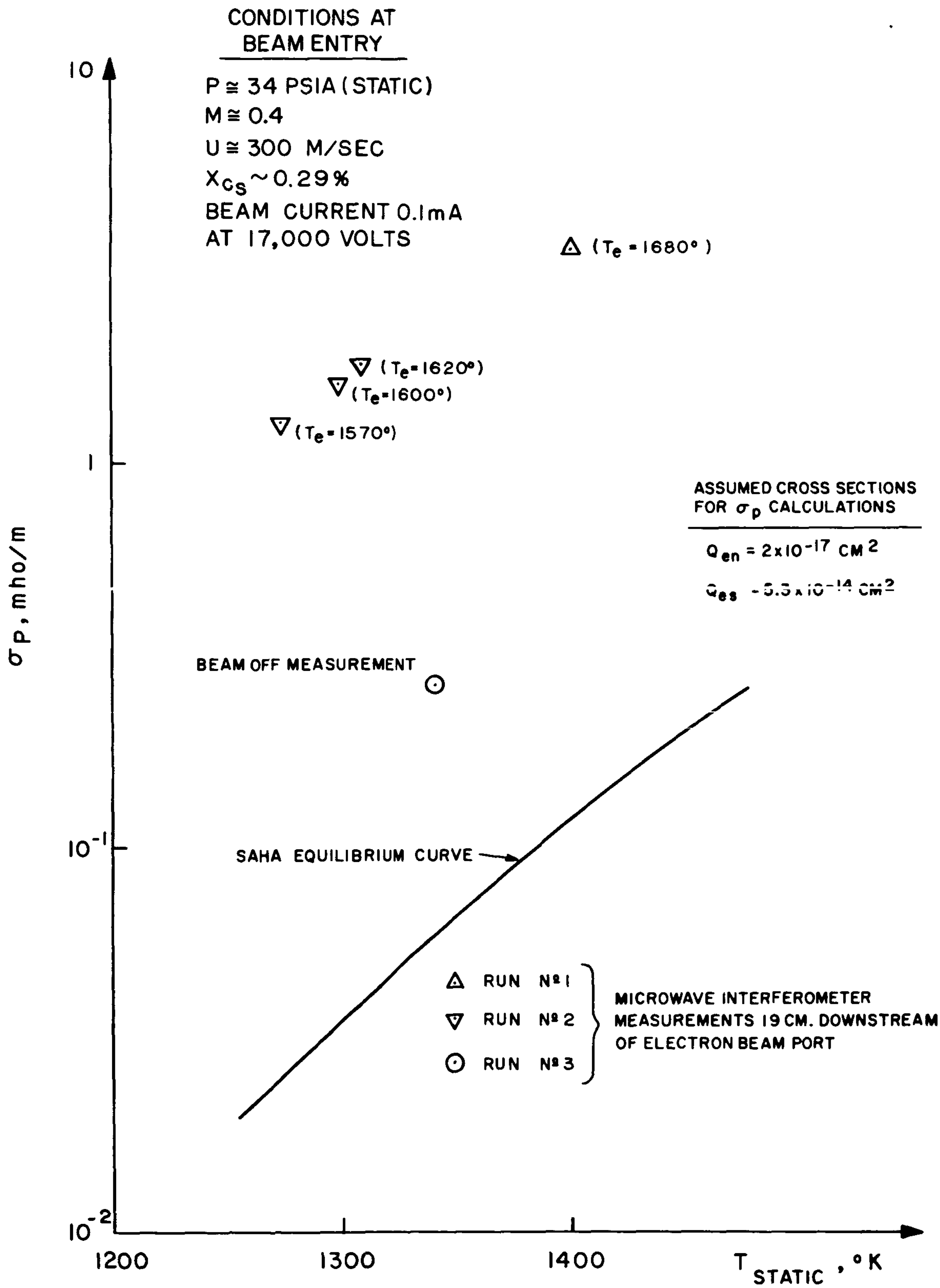

Figure 7. Electron Beam Enhancement of Conductivity

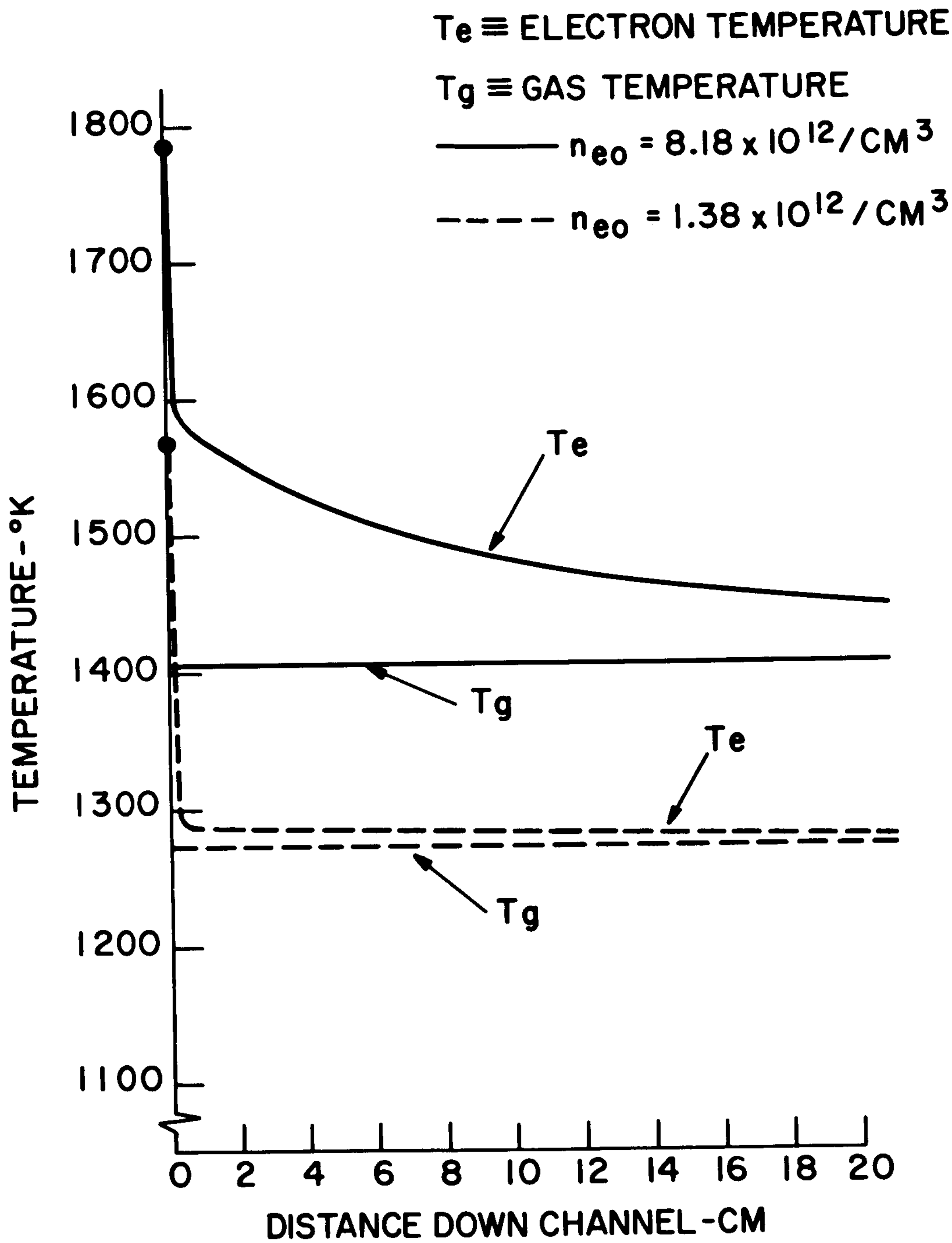

Figure 8A. Electron Temperature Variation Along Channel

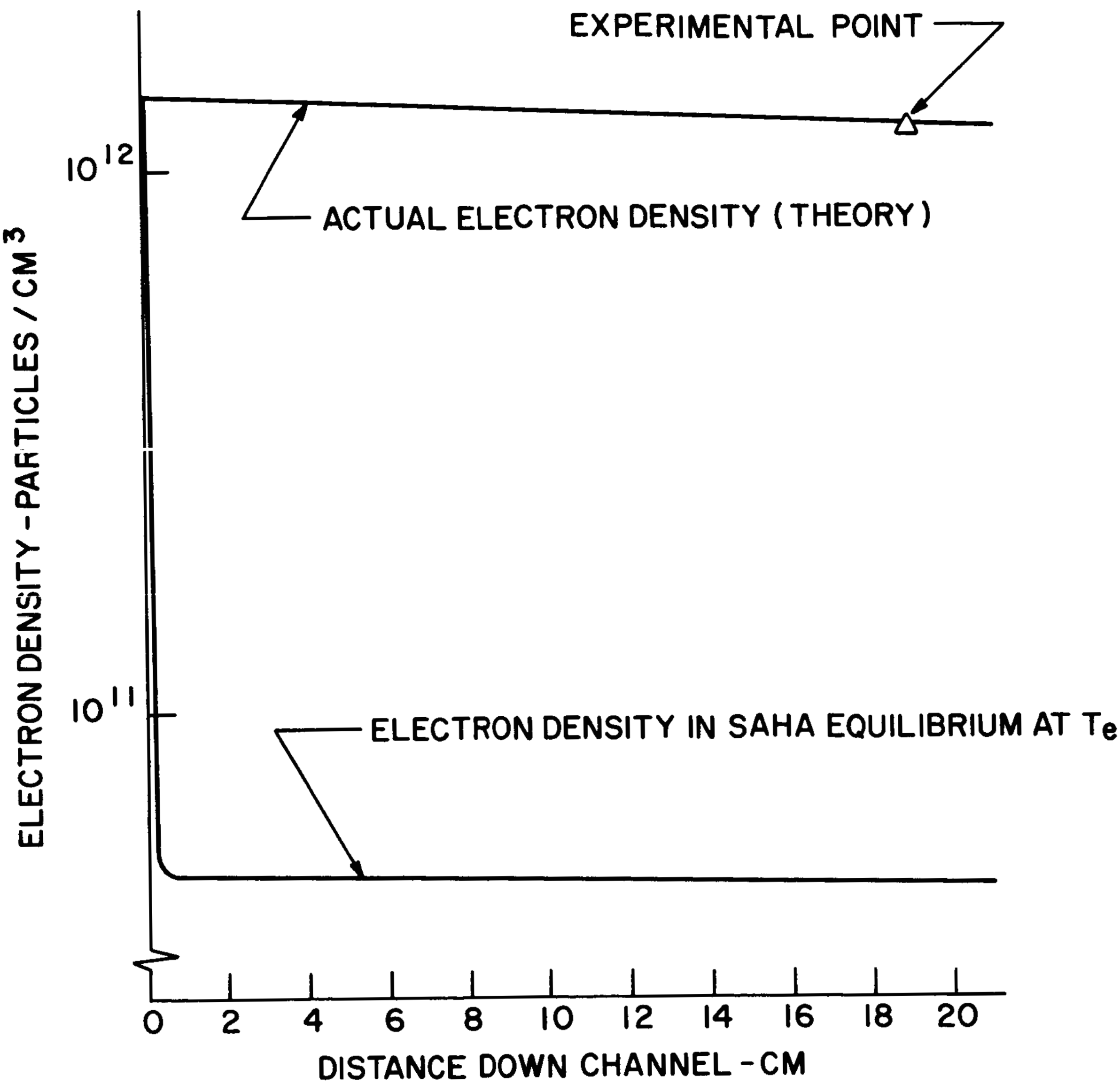

Figure 8B. Electron Density Decay Along Channel For $T_g = 1273^oK$

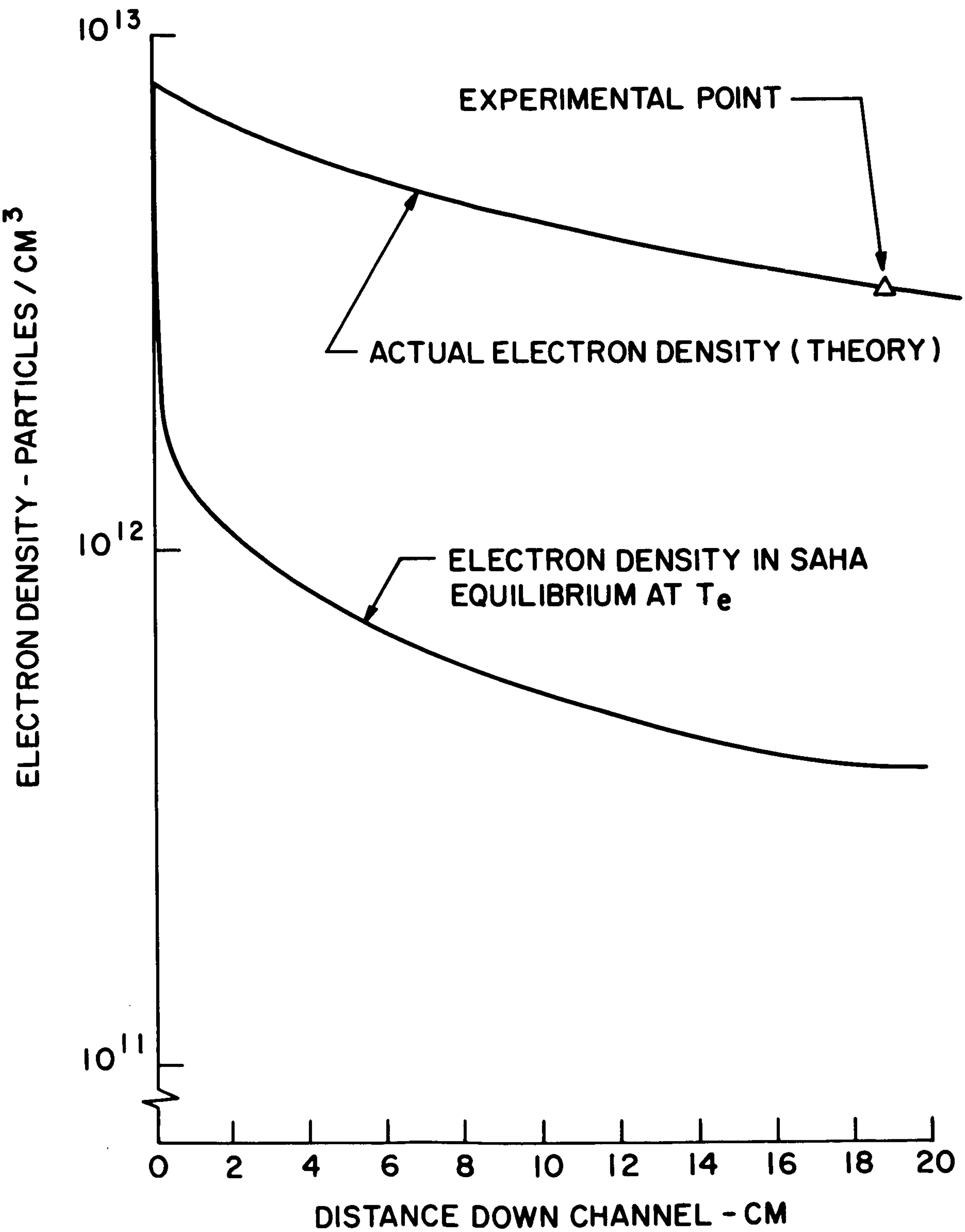

Figure 8C. Electron Density Decay Along Channel For $T_g = 1405^oK$

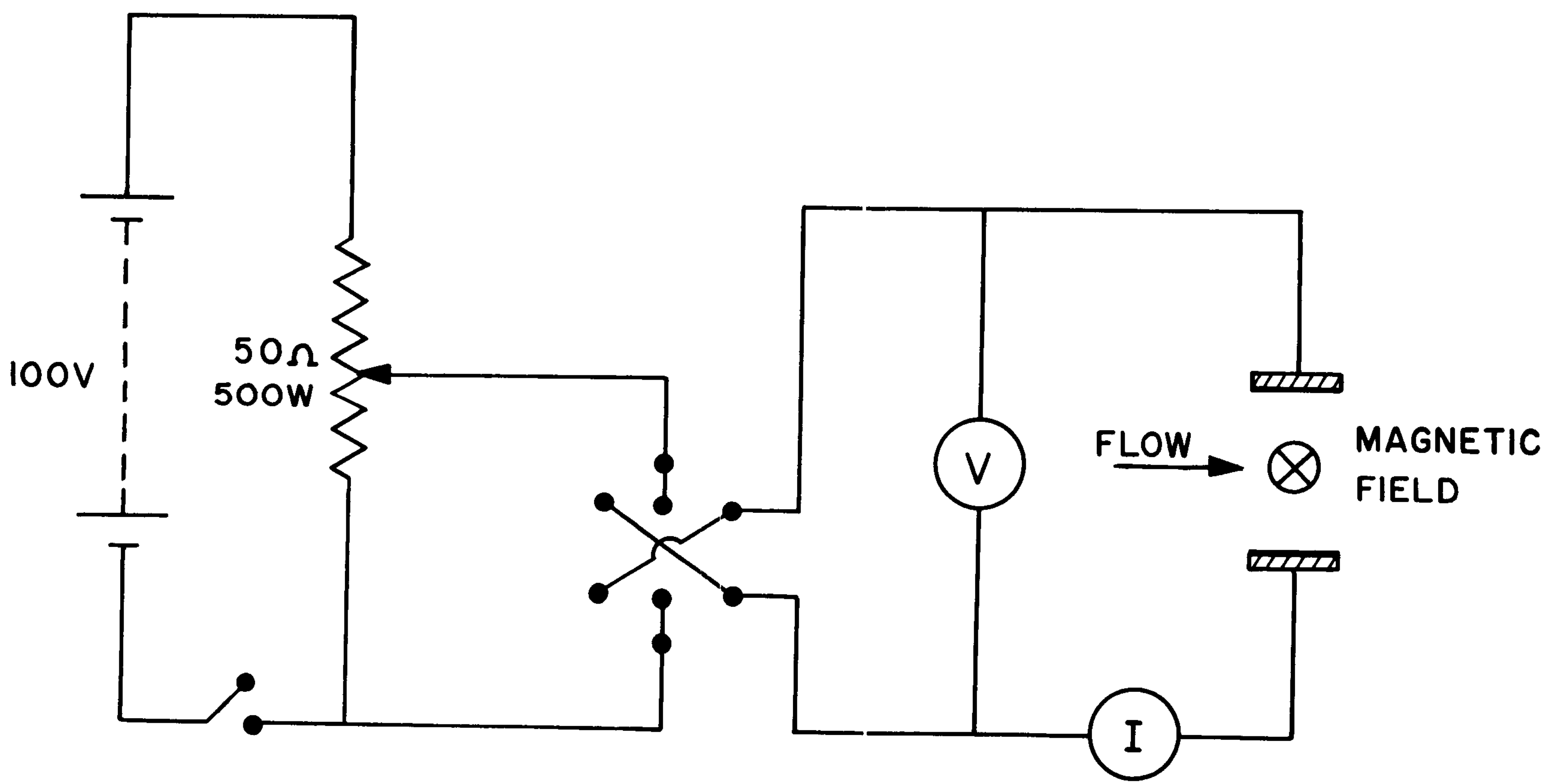

Figure 9. Circuit For Subsonic Applied Voltage Experiments With and Without Magnetic Field.

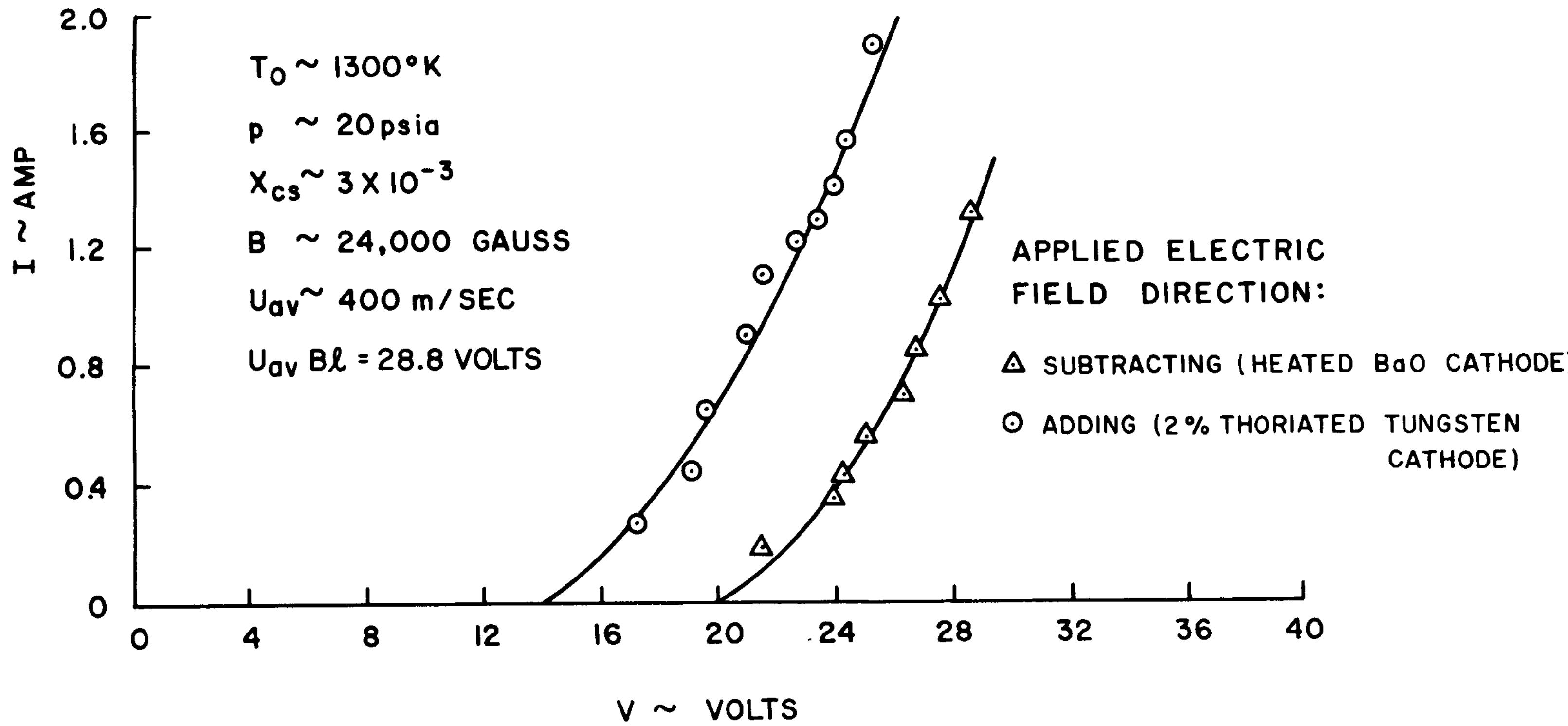

Figure 10. Cesium Seed With Applied Electric and Magnetic Fields

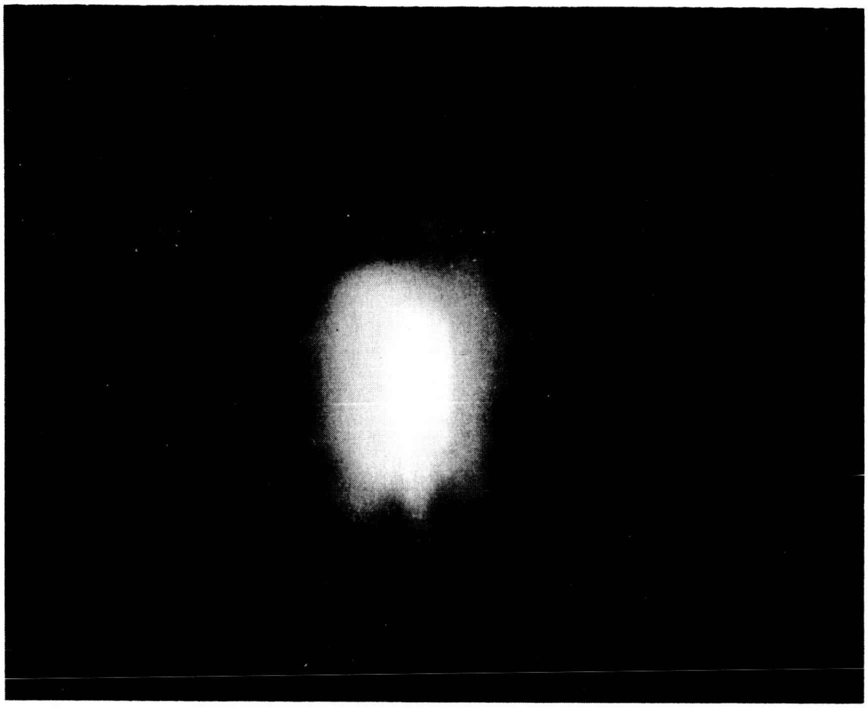

1. Low Current Density

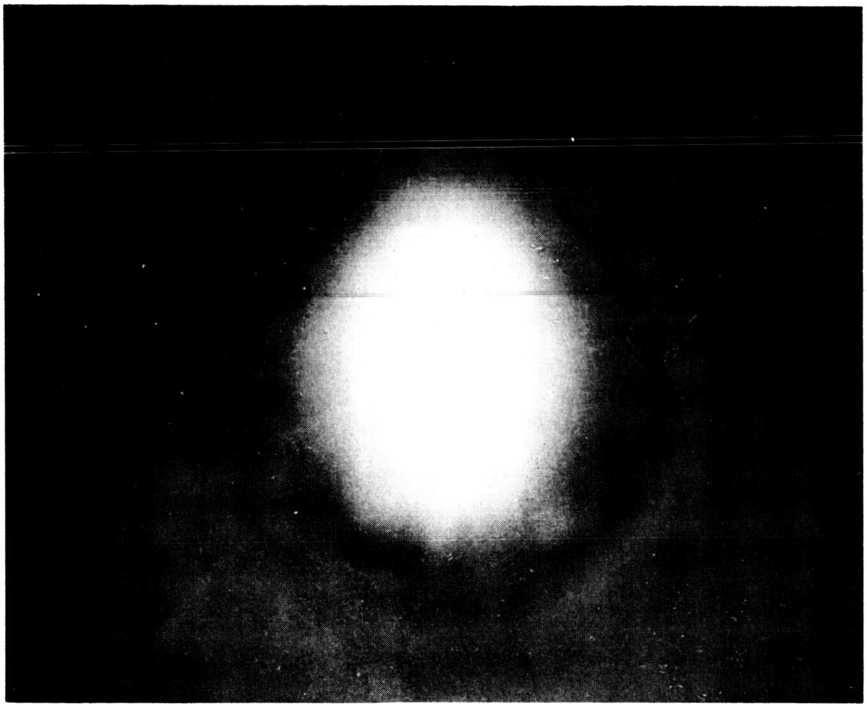

2. High Current Density

Figure 11. Typical Single Frame Cine Photographs of Glow Discharge in Cesium-Seeded Argon. $T_n \sim 1300$ deg. K, $X_{cs} \sim 0.3\%$

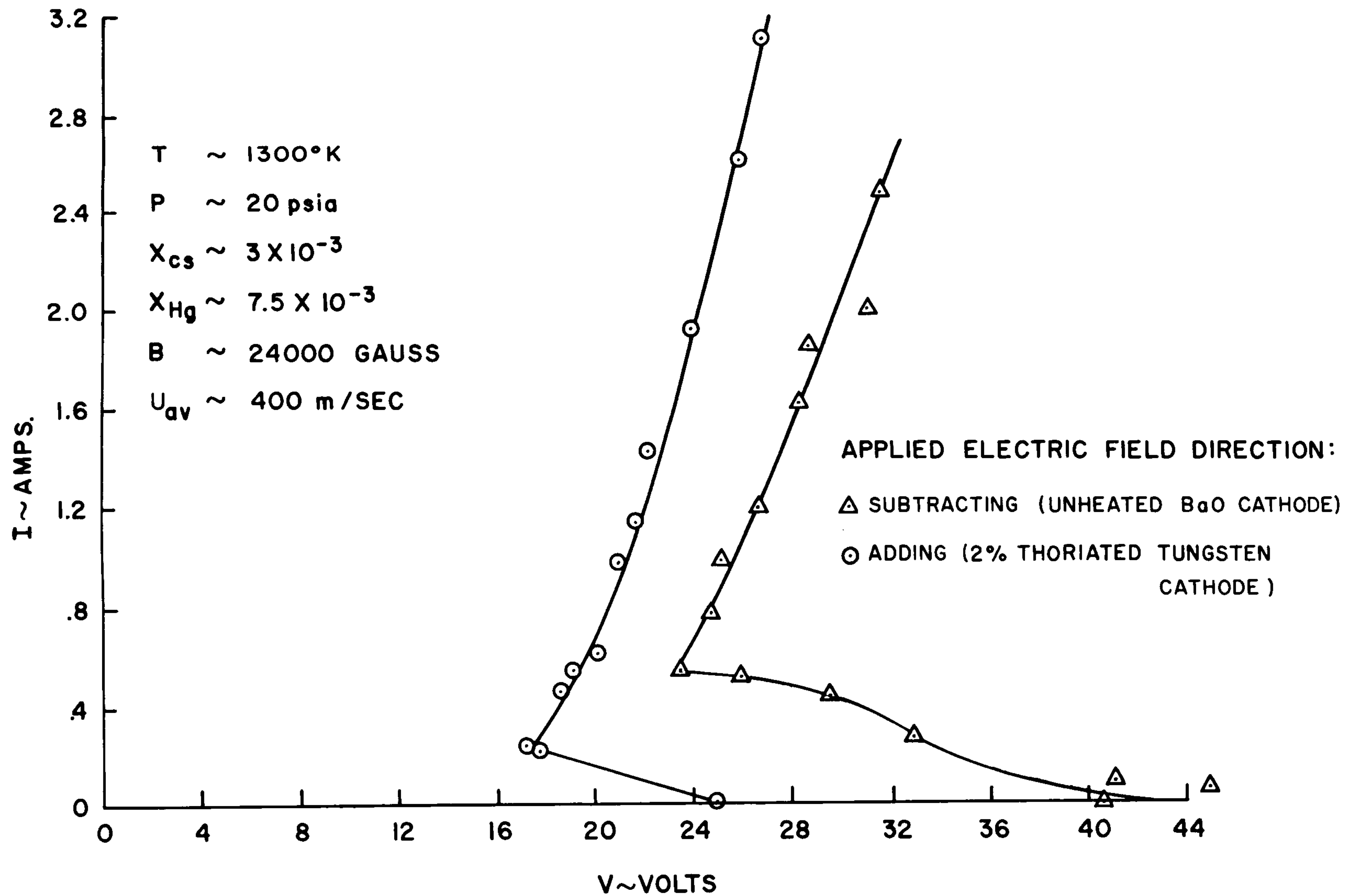

Figure 12. Metastable Seed Mixture With Applied Electric and Magnetic Fields

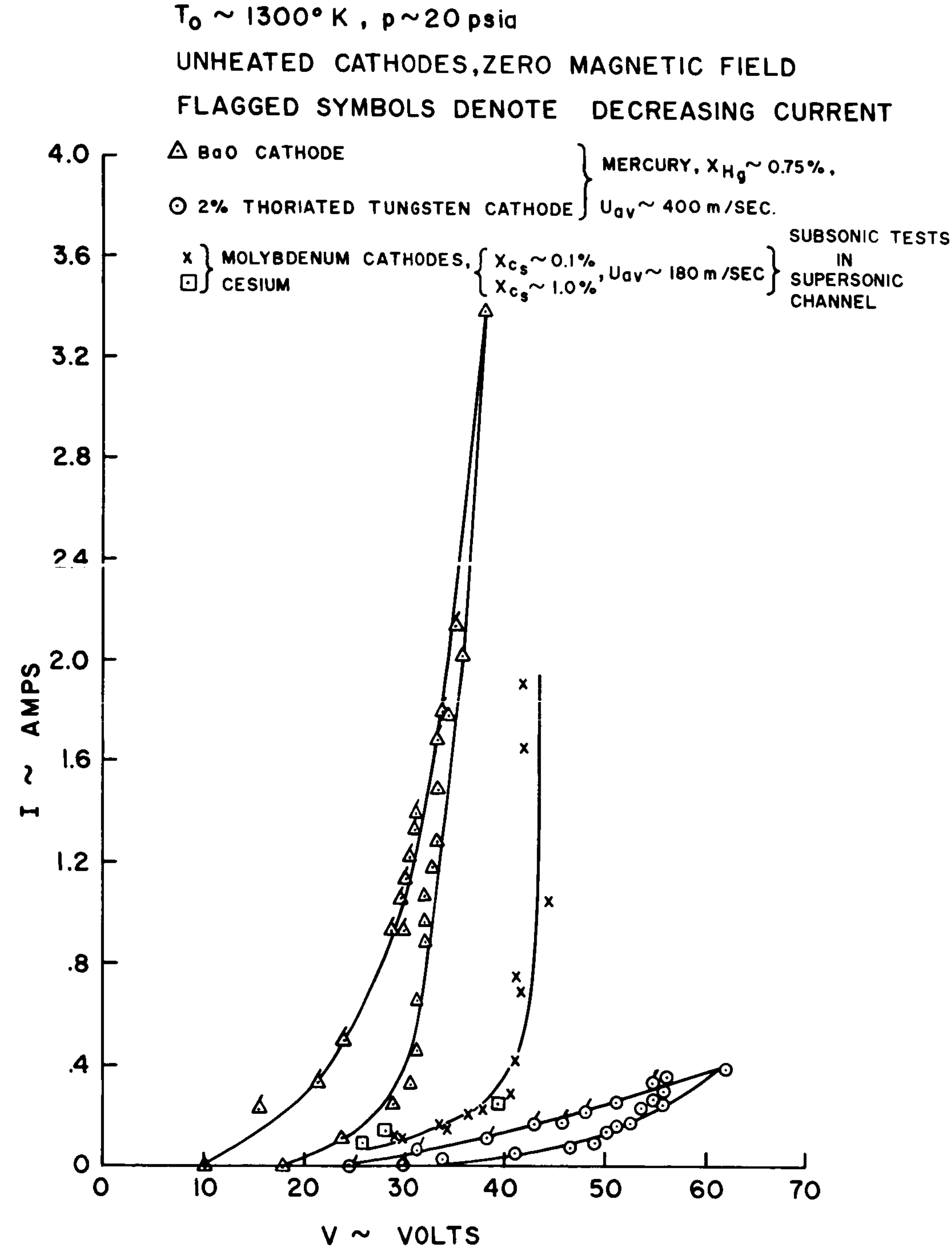

Figure 13. Applied Voltage vs. Current for Different Seed and Cathode Materials

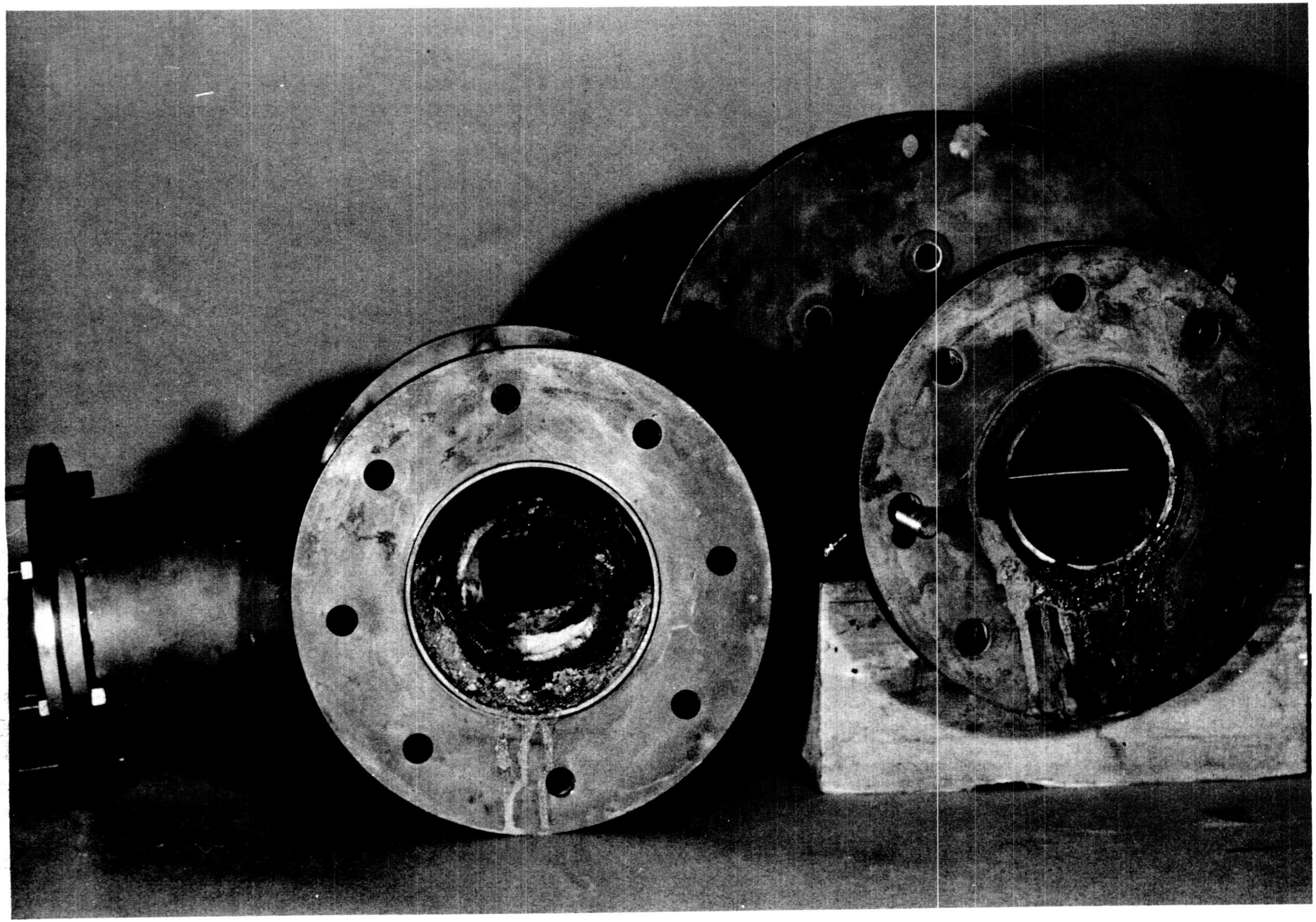

Figure 14. Seeding Station (right) and Adjacent Downstream Section (left) : Effect of Cesium Attack

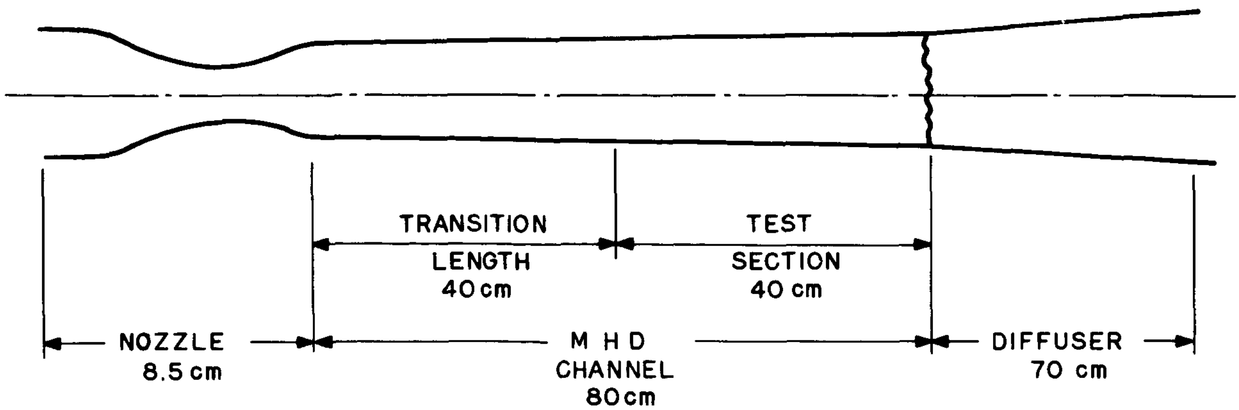

a) ASSEMBLY OF CHANNEL COMPONENTS

x	0	.281	.562	.843	1.124	1.405	1.846	2.348	2.913	3.539
y	.875	.879	.888	.902	.918	.938	.963	.986	.998	1.000

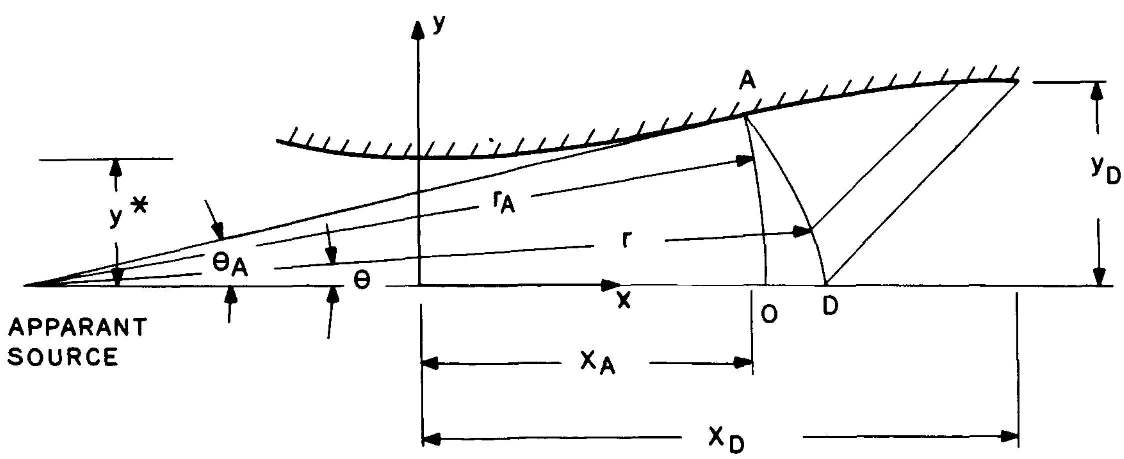

b) NOZZLE

Figure 15. Supersonic Channel Design

DISTRIBUTION LIST FOR

CONTRACT NAS3-6260

NASA Headquarters
FOB-10B
600 Independence Avenue, S. W.
Washington, D. C. 20546
Attention: RNT/James Lazar (2)
RPE/Dr. H. Harrison (1)
RNP/Dr. F. Schulman (2)
RNP/J. Lynch (1)
RNP/Dr. K. H. Thom (1)

Office of Naval Research
Power Branch (Code 429)
Washington, D. C. 20025
Attention: Dr. Ralph Roberts (1)
John Satkowski/Rm. 2509 (1)

USAF Office of Scientific Research
Washington, D. C. 20025
Attention: Dr. M. Slawsky (1)

AVCO/Everett Research Laboratory
2385 Revere Beach Parkway
Everett, Massachusetts
Attention: T. Brogan (1)

MHD Research Inc.
P. O. Box 1815
Newport Beach, California
Attention: Dr. V. H. Blackman (1)

Radio Corporation of America
Astro Electronics Division
Princeton, New Jersey
Attention: W. H. Hendel (1)

Melpar, Inc.
3000 Arlington Blvd.
Falls Church, Virginia
Attention: Dr. Roger C. Jones (1)

Westinghouse Astronuclear Laboratories
Pittsburgh 34, Pennsylvania
Attention: Mr. H. W. Szymanowski (1)
Electric Propulsion Laboratory

Giannini Scientific Corporation
3839 South Main Street
Santa Ana, California
Attention: Phillip J. Wyatt (1)

Aerospace Corporation
P. O. Box 95085
Los Angeles, California 90045
Attention: Library/Technical Documents
Group (1)

NASA-Lewis Research Center
21000 Brookpark Road
Cleveland, Ohio 44135
Attention: John H. DeFord (1)
J. H. Childs (1)
N. J. Stevens (4)
Bernard Lubarsky (2)
L. D. Nichols (1)
W. E. Moeckel (1)
Henry Sloan (1)
Reports Control Office (1)
Library (2)
Technology Utilization Office (1)

Aeronautical Systems Division
Flight Accessories Laboratory
Wright-Patterson AFB, Ohio
Attention: Robert Barthelemy APIE-2 (1)

Electrical Engineering Department
Massachusetts Institute of Technology
Cambridge 39, Massachusetts
Attention: Dr. J. Kerrebrock (1)
Prof. H. H. Woodson (1)

TRW Inc.,
TAPCO Group
23555 Euclid Avenue
Cleveland, Ohio 44117
Attention: W. C. David (1)

Republic Aviation Corporation
Plasma Propulsion Laboratory
Farmingdale, Long Island
New York 11735 (1)

Westinghouse R & D Center
Beulah Rd., Churchill Boro
Pittsburgh, Pennsylvania
Attention: Dr. E. V. Somers (1)

General Atomic Division
General Dynamics Corporation
P. O. Box 608
San Diego, California
Attention: Dr. M. O. Stern (1)

Martin-Marietta Corporation
Baltimore, Maryland 21203
Attention: Dr. Bienert (1)

Hughes Research Laboratories
Plasma Physics Department
3011 Malibu Canyon Road
Malibu, California
Attention: Mr. R. C. Knechtli (1)

Stanford University
M. E. Department
Stanford, California
Attention: Dr. R. H. Eustis (1)

Jet Propulsion Laboratory
4800 Oak Grove Drive
Pasadena, California 91103
Attention: D. G. Elliott (1)

AFWL
Kirtland AFB, New Mexico
Attention: WLPC/Capt. C. F. Ellis (1)

Mr. Thomas F. Stratton
University of California
Los Alamos Scientific Laboratory
P. O. Box 1663
Los Alamos, New Mexico 87544 (1)

American-Standard
Research Division
P. O. Box 2003
New Brunswick, New Jersey
Attention: E. Okress (1)

NASA Scientific & Technical Information Facility
Bethesda, Maryland, Box 5700
Attention: RQT-2448/NASA Representative (6)

The Garrett Corporation
Air Research Manufacturing Division of Phoenix
402 South 36th Street
Phoenix, Arizona (1)

CASE Institute of Technology
Engineering Division
University Circle
Cleveland, Ohio 44106
Attention: Dr. Eli Reshotko (1)